Modeling of high speed erosion with a morphological updating routine

Carlos Emilio Arboleda Chavez

Technische Universiteit Delft

Delft University of Technology

Challenge the future

Modeling of high speed erosion with a morphological updating routine

by

Carlos Emilio Arboleda Chavez

in partial fulfillment of the requirements for the degree of

Master of Science
in Dredging and Offshore Engineering

at the Delft University of Technology,
to be defended publicly February 22, 2017.

Supervisor:	Ir. J. C. Goeree	TU Delft, IHC
Thesis committee:	Prof. dr. ir. C. van Rhee,	TU Delft
	Dr. ir. M.J.B.M. Pourquie	TU Delft

This thesis cannot be made public until March 1, 2019

TU Delft Delft University of Technology

Contents

1 Acknowledgement **1**

2 Introduction **3**
2.1 Background . . . 3
2.2 Research aim . . . 4
2.3 Research Methodology . . . 4
2.4 Outline . . . 4

3 Governing equations of fluid motion **5**
3.1 Fluid model . . . 5
3.2 Turbulence model . . . 7

4 Sediment transport **9**
4.1 Suspended sediment transport . . . 9
4.1.1 Settling velocity and hindered settling . . . 9
4.2 Suspended sediment/sand-bed interaction . . . 11
4.2.1 Deposition and sedimentation velocity . . . 11
4.2.2 Threshold of motion . . . 13
4.2.3 Erosion . . . 15
4.3 Bed-load transport . . . 15

5 Numerical implementation of governing equations **17**
5.1 Discretization method: The finite volume method . . . 17
5.2 Fluid motion. . . . 18
5.2.1 Pressure-implicit with Separation of Operators (P.I.S.O) . . . 18
5.2.2 Boundary treatment for the velocity . . . 19
5.2.3 Boundary treatment for the pressure . . . 20
5.2.4 Boundary treatment for kinetic turbulent energy . . . 21
5.2.5 Boundary treatment for kinetic turbulent energy dissipation . . . 22
5.2.6 Boundary treatment for turbulent viscosity . . . 22
5.3 Sediment transport . . . 23
5.3.1 Implicit solution of sediment transport equation . . . 23
5.3.2 Boundary treatment of sediment transport . . . 23
5.4 Morphological routine and mesh handling . . . 24
5.4.1 Boundary treatment of mesh motion . . . 25

6 Settling test **27**
6.1 Experimental test. . . . 27
6.2 Numerical test . . . 28
6.2.1 Sediment as passive scalar . . . 28
6.2.2 Boussinesq approximation . . . 31
6.3 Summary . . . 34

7 High speed erosion test **35**
7.1 Experimental test. . . . 35
7.2 Numerical model setup . . . 36
7.2.1 The domain . . . 37

7.3 Result . . . 38
7.3.1 Erosion velocity . . . 38
7.3.2 Conductivity probes . . . 38
7.3.3 Bed height . . . 40
7.3.4 Velocity, concentration and turbulent eddy viscosity profiles . . . 41
7.3.5 Sediment volume conservation . . . 42

8 Conclusion **45**

Bibliography **47**

A Apendix A **49**

1
Acknowledgement

During this thesis, I had the privilege of being part of the Dredging Department of Delft University of Technology, while developing my scour model under the supervision of Prof.dr.ir. Cees van Rhee and Ir. J.C. Goeree. I would like to thank, my daily supervisor, Ir. J.C. Goeree, for all the help and valuable hindsight that he has provided me to finalize this project, Dr. Geert Keetels, for letting me assist him with the course CFD for Dredging and Offshore Engineering, Ir.Bas Nieuwboer, for letting me participate in his experimental research of particles behaviour inside the head of a cutter suction dredger in one of the flumes at the Hydraulics Laboratory of TU Delft, all the PhD. candidates in the Dredging department, for their contribution to this thesis in a way or another, and my friends.

Finally, I want to thank my family and specially my mother for all the support and patience.

2
Introduction

2.1. Background

Erosion is a phenomenon present in several industrial processes. In dredging, the jetting of sand in dragheads, erodes the sand-bed. In construction of offshore infrastructure such as wind turbines, oil and gas production units, marine pipelines, erosion of material near the foundations can put the stability of structures at stake. Furthermore, rivers or even tsunamis are some of the natural phenomena that can be cause of erosion.

This thesis will treat about fluid mechanics and sediment transport modelling. Sand-water mixtures can be modeled using the continuum approach if the chosen control volumes are big enough, meaning that the volume of a particle is much smaller than the volume of a cell. Leading to the use of the finite-volume method. The latter, allows a conservative assessment of the terms of the Navier-Stokes equations, if combined with the divergence theorem. Eases the implementation of boundary conditions and can easily be adapted to complex geometries. Using the continuum approach for modelling sediment transport, leads to consider the sediment as a volume fraction (volumetric concentration) being transported by the fluid. Furthermore, an Eulerian approach is preferred here to the Lagragian approach as it reduces the computational cost. Regarding sediment transport, a granular non-cohesive material (sand) is here considered.

Erosion is the removal of material of a sand-bed caused by viscous and turbulent stresses due to fluid motion. Bisschop et al. [1], distinguished two regimes for the pick-up function of saturated sand. On the one had erosion at low Shield's parameter, velocities of 0.5-$1 m.s^{-1}$, is dependent on the size and the density of the grains. On the other hand, high speed erosion creates a rearrangement in the structure of the sand-bed. The shearing of sand particles in the sand-bed, produces a rearrangement of sand particles, yielding to an increase of the void ratio in the sand-bed. This dilatant behaviour leads to a drop in the pressure in the interior of the sand-bed, inducing a hydraulic gradient. Water to flows towards the interior of the sand-bed, in order to fill the voids. The hydraulic gradient caused by the drop in pressure acts against the eroding forces, adding resistance to the erosion process. θ_{cr0}, also known as the Critical Shield's parameter, see [2], is the stability criterion and, accounts for the forces resisting to erosion. The implementation of this added resistance is formulated as a correction parameter to the Critical Shield's parameter as proposed by C. van Rhee [3], the corrected stability criterion is noted θ_{cr}. This formulation of the stability criterion takes into consideration the bulk properties of the sand-bed, its porosity and permeability, as well as the sand grain size and density.

High speed erosion of sand is present in applications as:

- Dredging
- Mining
- Trenching

OpenFOAM and foam-extend 3.2 are continuum mechanics library freely available. Unfortunately, the user is challenged by the diversity of the versions available and a high level C++ code. The version or flavour used here is the foam-extend 3.2 framework because a moving mesh routine is readily implemented.

2.2. Research aim

This research aim is to numerically model high speed erosion. Erosion is the removal of material from a surface. High speed erosion, other than removing material from a sand-bed, will produce a rearrangement of the sand particles inside the bed, therefore, adding an extra resistance to erosion. In order to determine the shear stresses that the fluid exerts on the sand-bed, the P.I.S.O algorithm is used. The balance of sediment in the sand-bed is assured by the moving mesh module, readily implemented in the foam-extend framework.

2.3. Research Methodology

The methodology implemented here consists first in a literature revue of the existing implementations of high speed erosion, erosion and scour problems. Inspired by the literature revue, implement and test the result of the model, by comparing the numerical solutions to 2 experimental tests. The first test will show the capabilities of the code in a settling test, then a high speed erosion test is studied.

2.4. Outline

The modelling of sand-bed using a moving mesh, updated depending on the removal or addition of sand, (also called morphological updating routine) has gained popularity. X. Lui [4] in 2008 and N. G. Jacobsen [5] in 2011, proposed codes for modelling of erosion and scour coupled with wave generation and free surface modelling based in the OpenFOAM framework. An application of the moving mesh approach is the modelling of hopper sedimentation proposed by C. van Rhee in 2002 [6]. In 2015, C. van Rhee, F. Bisschop at al. extended the approach proposed by C. van Rhee in 2002 and proved that the high speed erosion process can be modelled with a moving mesh.

Erosion is due to the stresses applied by the fluid on the sand-bed. These stresses are responsible of the resuspension of sand grains. The erosion rate is expressed by a pick-up function, the van Rijn pick-up function [7] is expressed as:

$$\Phi = 0.00033 D_*^{0.3} \left(\frac{\theta - \theta'_{cr}}{\theta'_{cr}} \right)^{1.5}$$

Here, θ is the Shield's parameter and is dependent on the fluid forces acting on the sand particles. As for θ_{cr} is the stability criterion and accounts for the forces resisting to erosion. In order to determine the forces being applied to the bed surface, the fluid behaviour needs to be modelled. The fluid is modelled by solving the Navier-Stokes equations in a discretized space.

In order to model the erosion process, the main equations that are numerically solved are:

- Mass conservation equation
- Momentum conservation equation
- Sediment transport equations
- Equation of mesh motion

The momentum conservation equation is determined using a pressure correction method, the P.I.S.O method is explained in section 5.2.1. Turbulence is modelled using Reynolds Averaged Navier Stokes (RANS) approach, because of its low computational cost and applicability to 2D problems. A 2-equations model, the k-ϵ approach determines the turbulent eddy viscosity (section 3.2) accounting for the dissipation of energy due to turbulent mixing.

The sediment transport is composed by suspended sediment transport and bed-load transport. The suspended sediment transport is presented in section 4, it is solved by using an advection-diffusion relation. The interaction between the sand-bed and the suspended sediment, is depicted by the erosion and deposition phenomena. The mathematical formulation of erosion and deposition is discussed in sections 4.2.1 and 4.2.3. Finally, the bed-load transport is presented in section 4.3.

3

Governing equations of fluid motion

In this section, the governing equations of fluid motion are presented. In section 3.1, the well known Navier-Stokes equations are introduced in their general conservative form, the incompressibility hypothesis is formulated and the Boussinesq approximation to account for the momentum exchange between sediment and fluid is discussed. Finally, the turbulence model is depicted in subsection 3.2.

3.1. Fluid model

The Navier-Stokes equations (from now on "NS equations" for simplicity), are a set of coupled equations that depict the motion of fluids. The three equations that conform the NS set of equations are, namely, the mass conservation equation 3.1, also called continuity equation, the momentum conservation equation 3.2 and the energy conservation equation. The aforementioned set of equation is presented in their differential conservative form for an Eulerian reference frame hereafter. The energy equation is omitted.

Mass conservation equation:

$$\frac{\partial \rho}{\partial t} + \vec{\nabla} \cdot (\rho \vec{u}) = 0 \tag{3.1}$$

Momentum conservation equation:

$$\frac{\partial \rho \vec{u}}{\partial t} + \vec{\nabla} \cdot (\rho \vec{u} \otimes \vec{u}) = -\vec{\nabla} p + \vec{\nabla} \overline{\overline{\tau}} + \rho \vec{f} \tag{3.2}$$

Where:
ρ, the density of the fluid considered.
p, the pressure.
$\vec{u}$, the velocity.
t, the time.
$\vec{f}$, the body forces.
$\overline{\overline{\tau}}$, the shear stress tensor.

The density of the slurry (sand-water mixture), ρ_m, can be expressed as a function of the volumetric concentration, c, the density of sand, ρ_s and the density of water, ρ_w, as follows:

$$\rho_m = c\rho_s + (1-c)\rho_w \tag{3.3}$$

ρ_m can be decomposed in an average and a perturbation:

$$\rho_m = < \rho_m > + \rho'_m \tag{3.4}$$

From equations 3.3 and 3.4, we can identify:

$$< \rho_m >= \rho_w \tag{3.5}$$

and,

$$\rho'_m = c(\rho_s - \rho_w) \tag{3.6}$$

The mass conservation equation can be formulated for the slurry as follows:

$$\frac{\partial \rho_m}{\partial t} + \vec{\nabla} \cdot (\rho_m \vec{u}) = 0 \tag{3.7}$$

P. Wesseling in [8], explained that for small variation of the density ($\frac{\rho'_m}{<\rho_m>}$«1), the flow can be considered incompressible by neglecting this fluctuations. A concrete example of an incompressible fluid with a non-constant density is salty water. Therefore, if the temporal and spatial variation of the slurry density are considered negligible. The mass conservation equation yields the continuity condition for incompressible flows:

$$\vec{\nabla} \cdot \vec{u} = 0 \tag{3.8}$$

And the momentum conservation reads:

$$\frac{\partial \vec{u}}{\partial t} + (\vec{u} \cdot \vec{\nabla})\vec{u} = -\frac{\vec{\nabla} p}{\rho_m} + \nu \nabla^2 \vec{u} + \vec{f} \tag{3.9}$$

The mixture is subjected to Earth's gravity field. As stated previously, the density of the mixture is not constant, the inhomogeneous presence of sediment in the fluid will yield gravity/density induced body forces. This body forces are accounted in the term $\vec{f}$ in the r.h.s of equation 3.9. This body forces can be expressed as follows

$$\vec{f} = \frac{\rho_m - \rho_w}{\rho_w} \vec{g}$$

if:

$$\rho_k = \frac{\rho_m - \rho_w}{\rho_w}$$

then:

$$\vec{f} = \rho_k \vec{g}$$

The Boussinesq approximation neglects the impact of density variations in all the terms of the momentum equation 3.9, except for the body forces. Furthermore, this approximation neglects the interactions between sand particles.

In figure 3.1, the relation between the volume fraction and the density of the resulting mixture has been plotted. Remark that the mixture density can vary from 1000 kg/m^3 for clear water to 2000 kg/m^3 for a saturated sand-bed, which represent 100% variation of the density. This large variation of density of the mixture makes it possible to chose different approaches to account for the interaction between the fluid and the sediment in terms of momentum exchange. For very low concentrations, c≈0, considering sand as a passive scalar can lead to satisfactory results. The formulation of the incompressibility can be made if:

$$\frac{\rho'_m}{< \rho_m >} << 1$$

From equation 3.3, we can write:

$$\frac{c(\rho_s - \rho_w)}{\rho_w} << 1$$

$$c(\frac{\rho_s}{\rho_w} - 1) << 1$$

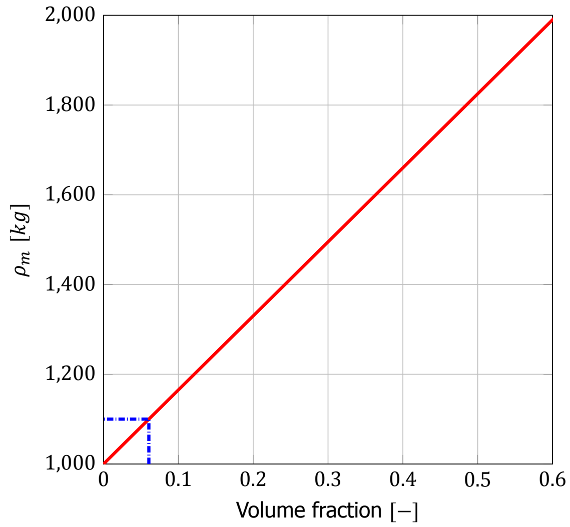

Figure 3.1: Representation of the mixture density with respect to the volume fraction of sand (ρ_{sand} = $2650 kg/m^3$)

If $\rho_s = 2650kg/m^3$ and $\rho_w = 1000kg/m^3$ then:

$$c << 0.625$$

A concentration of c=0.0625 leads to a variation of the mixture density of 10%, this is considered for this work as the upper limit of validity for the incompressibility hypothesis and the Boussinesq approximation. For higher concentration, the exchange of momentum between the sediment and the fluid is non-negligible and the incompressibility hypothesis does not stand, therefore, more elaborated fluid/sediment model should be used, for example, the continuous flow model proposed by C. van Rhee and J.C. Goeree [9]. The concentrations studied in the settling test are of 0.2 and 0.3, as for the erosion test, the concentration can go up to 0.45. These concentrations are higher than 0.0625, thus, the continuous flow model should be used. For simplicity, the Boussinesq approximation is used instead in this work.

3.2. Turbulence model

Turbulence has an important role in erosion, bed-load transport and resuspension of sediment, as shown in [10] and in [11]. A Reynolds Averaged Navier-Stokes (R.A.N.S) method is used, with a standard two equation k-ϵ model. The velocity can be decomposed into time averaged values ($< \vec{u} >$) and a perturbation ($\vec{u}'$). This is called the Reynolds decomposition:

$$\vec{u} =< \vec{u} > +\vec{u}'$$

$$p =< p > +p'$$

$$\vec{f} =< \vec{f} > +\vec{f}'$$

The decomposed quantities are included in the incompressible NS equations, the subscripts here refer to the reference base vectors.
The continuity equation:

$$\frac{\partial < \vec{u} >_i}{\partial x_i} = 0 \tag{3.10}$$

The momentum equation:

$$\frac{\partial < \vec{u} >_i}{\partial t} + < \vec{u} >_j \frac{\partial < \vec{u} >_i}{\partial x_j} + \left\langle \vec{u}'_j \frac{\partial \vec{u}'_i}{\partial x_j} \right\rangle =< \vec{f} >_i - \frac{1}{\rho} \frac{\partial < p >}{\partial x_i} + \nu \frac{\partial^2 < \vec{u} >_i}{\partial x_i \partial x_j}$$

Rearranging and averaging in time yields:

$$\rho < \vec{u} >_j \frac{\partial < \vec{u} >_i}{\partial x_j} = \rho < \vec{f} >_i + \frac{\partial}{\partial x_j}\left[- < p > \delta_{ij} + 2\mu < S_{ij} > -\rho < \vec{u}_i'\vec{u}_j' >\right]$$

Where:

$$< S_{ij} >= \frac{1}{2}\left(\frac{\partial < \vec{u} >_i}{\partial x_j} + \frac{\partial < \vec{u} >_j}{\partial x_i}\right)$$

δ_{ij}, the delta Kronecker.
μ, is the dynamic viscosity of the fluid.
Note that here the indexes (i,j) represent the components.

The term $\rho < \vec{u}_i'\vec{u}_j' >$ is called the Reynolds stresses. In order to determine this quantity, Boussinesq proposed in 1877 the concept of eddy viscosity. This concept considers that the turbulent shear stresses are proportional to the velocity gradient as for the viscous stresses in a laminar flow.

$$\rho < \vec{u}_i'\vec{u}_j' >= -\rho\nu_t\frac{\partial \vec{u}_i}{\partial x_j}$$

The turbulent eddy viscosity (ν_t) accounts for the dissipation of energy due to turbulence and it is a property of the flow field and not the fluid.

An expression for the turbulent eddy viscosity is:

$$\nu_t = C_\mu\frac{k^2}{\epsilon} \tag{3.11}$$

This turbulent viscosity is added to the kinematic viscosity of the fluid ν. The effective viscosity ν_{eff} can then be formulated as follows:

$$\nu_{eff} = \nu_t + \nu$$

The k-ϵ model introduces a new set of two coupled equations, where k represents the turbulent kinetic energy and ϵ the dissipation rate of turbulent kinetic energy.

$$\frac{\partial k}{\partial t} + \vec{\nabla}\cdot(k\vec{u}) = \vec{\nabla}\cdot(\frac{\nu_t}{\sigma_k}\vec{\nabla}k) + \frac{P}{\rho} - \epsilon \tag{3.12}$$

$$\frac{\partial \epsilon}{\partial t} + \vec{\nabla}\cdot(\epsilon\vec{u}) = \vec{\nabla}\cdot(\frac{\nu_t}{\sigma_\epsilon}\vec{\nabla}\epsilon) + C_{\epsilon 1}\frac{P\epsilon}{\rho k} - C_{\epsilon 2}\frac{\epsilon^2}{\rho k} \tag{3.13}$$

where:

Table 3.1: Constant values for turbulent calculations

C_μ	σ_k	σ_ϵ	$C_{\epsilon 1}$	$C_{\epsilon 2}$
0.09	1.00	1.3	1.44	1.92

The turbulent eddy viscosity (ν_t), is used as the diffusivity in the sediment transport equation. The K-ϵ model used in Foam-extend 3.2 does not include a buoyancy production term.

4
Sediment transport

The sediment transport for this work is decomposed in three main components, namely, the suspended sediment transport, suspended sediment/bed interaction and the bed-load transport. The suspended sediment transport formulates the motion of sediment particles when governed by gravity and fluid forces. The expression used to determined the motion of the suspended particles is the transport equation 4.1. The suspended sediment/bed interaction is mathematically formulated by the erosion and the deposition rate. Finally, the bed-load transport is a transport from the sand-bed to the sand-bed. It is determined by numerically solving the partial differential equation of a curves plane in the 3D space, see equation 4.27.

4.1. Suspended sediment transport

Suspended sand is transported by the fluid and is here considered as a continuum. This phenomenon is represented mathematically by an advection-diffusion equation as presented in Eq.4.1. The diffusivity coefficient is taken as the turbulence viscosity. The grains of sand are considered uniform, meaning that multiple fraction are not implemented in this model.

$$\frac{\partial c}{\partial t} + \vec{\nabla} \cdot [c(\vec{u} + \vec{w}_{set})] = \vec{\nabla} \cdot (\nu_t \vec{\nabla} c) \tag{4.1}$$

Where:
c, the voumetric concentration of sediment.
$\vec{u}$, is the fluid velocity vector.
$\vec{w}_{set}$, is the hindered settling velocity vector.
ν_t, the turbulent eddy viscosity.
Note that the sediment is advected by the velocity $\vec{u} + \vec{w}_{set}$, which is the velocity of a grain of sand being transported by a flow with a velocity $\vec{u}$ and its hindered settling velocity $\vec{w}_{set}$. The hindered settling velocity $\vec{w}_{set}$ accounts for the impact of the gravity on the grains of sand and the influence of concentration. This is explained in the next section.

4.1.1. Settling velocity and hindered settling

If the bulk density of sediment is higher than the density of water ($\rho_s > \rho_w$), then, suspended grains of sediment will sink. This phenomenon is called settling, thus, the velocity at which particles settle is called the settling velocity. In this work, the expression for the settling velocity of a single particle of sand is determined using the formulation presented by Ferguson and Church [12].

$$w_0 = \frac{\Delta g d^2}{C_1 \nu + \sqrt{0.75 C_2 \Delta g d^3}} \tag{4.2}$$

Δ, the submerged specific density.
g, the gavitational acceleration.
d, the grain size diameter, here the D_{50}.

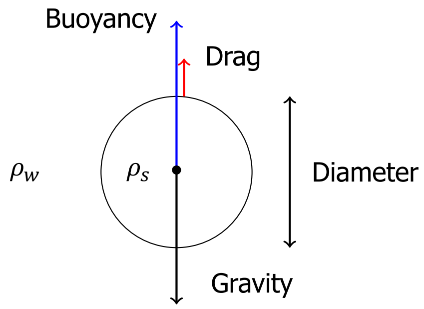

Figure 4.1: Forces acting on a single idealized grains of sand

w_0, the terminal settling velocity.
ν, the fluid viscosity.
C_1 and C_2 can take different values depending on the shape of the particles studied. C_1=18 and C_2=0.4 are used for smooth spheres. For sand grains of random shapes, C_1=18 and C_2=1.0 are used. The advantage of using this equation for the settling velocity of sand grains is that it is valid for a large range of Reynolds numbers [12].

The settling of multiple particles, interactions between particles and their disturbance of the fluid need to be considered. The settling of multiple particles will produce upward flow. The settling velocity will be reduced by the increased drag due to this upward flow. This effect is called hindered settling, a well known semi-empirical relation to estimate the settling velocity was proposed by Richardson and Zaki [13]:

$$\frac{w'_{set}}{w_0} = e^n \tag{4.3}$$

where:
e=1-c, is the voidage ratio.
c, the concentration.

Furthermore, if the velocity of a particle is small compared to the velocity of the fluid and for small particle Reynolds number, Mirza and Richardson (1979)[14], stated that to assess the relative settling velocity of a particle with respect to the fluid, the following formula should be used:

$$\frac{w_{set}}{w_0} = e^{n-1} \tag{4.4}$$

where:

$$w_{set} = \frac{w'_{set}}{e} \tag{4.5}$$

In 3D coordinates, if $\vec{z}$ is in the upward direction:

$$\vec{w}_{set} = (0, 0, -w_{set})$$

n, the exponent, was formulated as a function of the particle's Reynold number by Rowe [15]. The particle's Reynold number is defined as $Re_p = \frac{w_0 d}{\nu}$.

$$n = \frac{4.7 + 0.41 Re_p^{0.75}}{1 + 0.175 Re_p^{0.75}} \tag{4.6}$$

In fig. 4.2, the hindered settling velocity has been plotted as function of the concentration of sediment. The settling velocity of a single particle with a diameter of d=125μm is $w_0 = 0.011\ m.s^{-1}$. It's possible to visualize an important reduction of the fall velocity because of hindered settling. For a concentration close to 0, the fall velocity is close to the settling velocity of a single particle. For a concentration of sediment of 0.1, the fall velocity is reduced to $w_{set} = 0.007\ m.s^{-1}$ and for a concentration of 0.6 the fall velocity is close to 0. After some test, results using the formulation of Eq. 4.3 present better results in the settling test. This formulation is then kept for the erosion test.

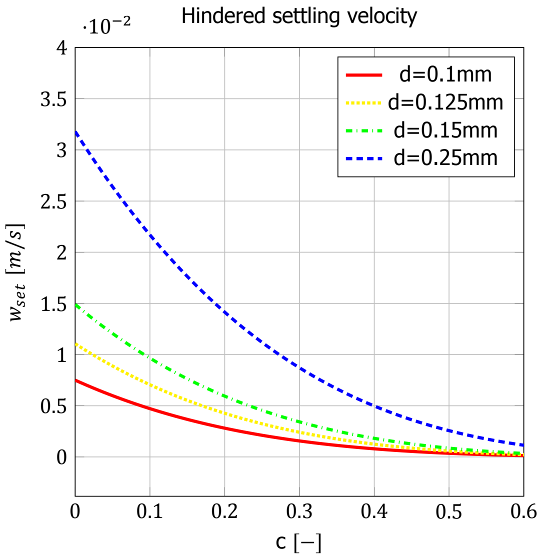

Figure 4.2: Impact of the concentration on the fall velocity of particles for different particle size. The settling velocity is determined with relation 4.2.

4.2. Suspended sediment/sand-bed interaction

In this subsection 3 processes are explained. First, the deposition of sediment in a bed, then, the erosion of a sand bed, and finally, the intra-bed mass exchange. These processes can be expressed as the Exner equation 4.7, proposed by Austrian meteorologist and sedimentologist Felix Maria Exner. This expression was presented in the works of Exner, see [16] and [17]. It has been used in similar works and has been expressed in the following manner, by X. Liu [4] and N.G. Jacobsen [5]:

$$\frac{\partial \eta}{\partial t} = \frac{1}{n_0 - 1}[-\nabla \cdot \vec{q}_b + S - E] \tag{4.7}$$

where:
η, represents the bed elevation.
$\nabla \cdot \vec{q}_b$, the bed load transport or sediment flux.
S, the rate of deposition of material in the bed.
E, the rate of erosion of bed due to the viscous and turbulent forces applied to the bed.
n_0, the sand-bed porosity. The concentration of the bed is then $c_{bed} = 1 - n_0$

The Exner equation is the formulation of the mass balance between the bed and the suspended sediment. The mass balance is translated in the Exner equation by the evolution of the bed height ($\frac{\partial \eta}{\partial t}$). In this work, the contributions of sedimentation and erosion(S, E) of the Exner equation are assessed using the sedimentation velocity concept. The deposition (S) represents the amount of sand settling that has reached the bed, and it is explained in the following section. The erosion (E) accounts for the quantity of materials being removed from the bed by the flow due to viscous and turbulent stresses. These stresses are also responsible for an intra-bed transfer of sediment, the bed-load ($\nabla \cdot \vec{q}_b$). The bed-load term can take into consideration various phenomena as saltation or rolling of sand grains, sliding of sediment, etc... For more information about bed-load transport, the reader is referred to the work of van Rijn [18]. As stated previously the erosion and bed-load are both linked to the viscous and turbulent stresses. The notion of incipient motion is the key to understand the bed physics. This notion is explained in section 4.2.2.

4.2.1. Deposition and sedimentation velocity

The settling of sand grains is due to the action of gravity. These settling particles that have reached the bottom will add mass to the sand bed. In this work, the interface fluid-bed, is represented by a moving boundary. The moving boundary adapts the height of every point depending on the balance of settled/eroded material at the time step. The deposition rate can be seen as the quantity of material

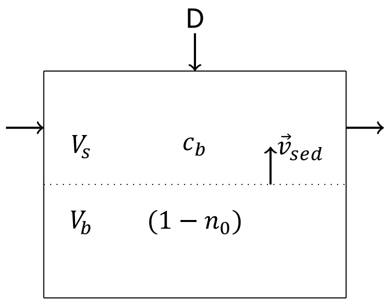

Figure 4.3: Figure representing a control volume near the settled bed. Source: On the sedimentation process in a Trailing Suction Hopper Dredger, 2002, van Rhee C. [6]

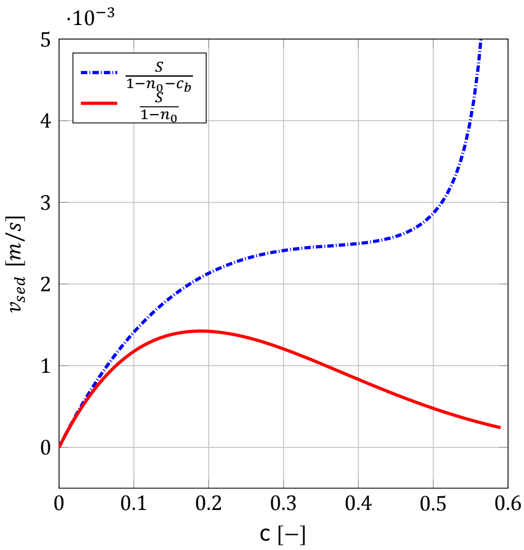

Figure 4.4: Comparison between 2 formulations of the sedimentation velocity for a particle diameter d=125e-6m

passing from the fluid domain through the sand-water interface. The deposition flux also called settling flux by van Rhee [6] can be expressed in the following fashion:

$$S = \rho_s c_b [\vec{w}_{set} \cdot \vec{N}] \tag{4.8}$$

ρ_s, the density of sand.
$\vec{N}$, the unit normal to the boundary
c_b, the near bed concentration From this settling flux, it is possible to define the sedimentation velocity. The sedimentation velocity as defined by van Rhee [6] is: the vertical velocity of the bed-water interface.

$$\vec{v}_{sed} \cdot \vec{N} = \frac{S}{\rho_s(1 - n_0 - c_b)} \tag{4.9}$$

This formulation of the sedimentation velocity gives an indication on the velocity of the bed when only deposition is present with no lateral transport of sediment. For more information about the derivation of this quantity, the reader is referred to the book of C. van Rhee [6]. As explained in the latter, $\vec{v}_{sed}$ has a term accounting for the near bed concentration, c_b, in the denominator, not including this term yield a large error when computing high concentration settling, see figure 4.4. Equation 4.9 is a simplified version of the sedimentation velocity, not accounting for the erosion. In order to account for the erosion flux explained in section 4.2.3, the sedimentation velocity has to be modify. The erosion rate, presented in further sections, is here included in equation 4.9.

$$\vec{v}_{sed} \cdot \vec{N} = \frac{S - E}{\rho_s(1 - n_0 - c_b)} \tag{4.10}$$

Note that the velocity is called sedimentation velocity, but if the erosion flux is higher, then, this quantity could be named the erosion velocity. For simplicity, this quantity is referred as sedimentation velocity. As stated previously in this section, $\vec{v}_{sed}$ is the velocity of the bed, calculated from the balance of the erosion/deposition fluxes. The bed height can therefore be calculated in an explicit manner as follows:

$$\frac{\partial \eta}{\partial t} = \vec{v}_{sed} \cdot \vec{N} \tag{4.11}$$

The erosion flux needs to be determined in order to have a full expression of the sedimentation velocity, but first, lets have a look at the notion of incipient motion.

4.2.2. Threshold of motion

The threshold of movement is defined as, the moment at which the motion of a particle at the bed starts. The forces acting on a bed particle are separated into resisting forces and driving forces. In the driving forces we can account the fluid forces, in other words the lift and the drag. As for the resisting forces acting on a settled particle it's possible to name the weight and the friction between particles. As stated previously the threshold of motion is defined as the instant when the driving forces are in static equilibrium with resisting forces. The erosion process will occur when the particles get into suspension. In the bed-load transport process, depending on the shear velocity the transport mode of particles would be different. The sediment transport mechanism can go from saltation for high shear velocities to sliding and rolling for lower shear velocities. In order to assess the state of the forces acting on a particle, we need an indicator. The indicator for the state of the forces acting on the bed surface particles is the Shield's parameter or adimensional shear, which was expressed by A. Shield [2] as:

$$\theta = \frac{u_*^2}{\Delta g D} \tag{4.12}$$

Where the friction velocity, u_*, can be defined by the well known law of the wall:

$$\frac{U_p}{u_*} = \frac{1}{\kappa} ln\left(\frac{32 y_p}{k_s}\right) \tag{4.13}$$

Where:
k_s, the bed roughness height
κ, the von Kármán constant.
U_p, the velocity at the wall nearest cell.
y_p, the distance between the boundary and the first cell center.

The log law of the wall, depicts the logarithmic behaviour of the averaged velocity distribution of a fluid in a turbulent flow at a $y^+ > 30$ of a wall. The relation between the wall shear stress and the friction velocity is:

$$u_*^2 = \frac{\tau_b}{\rho_m} \tag{4.14}$$

The shear stress in a turbulent flow can be expressed by equating 4.13 and 4.14:

$$\tau_b = \frac{\rho_m U_p^2}{\left(\frac{1}{\kappa} ln\left(\frac{32 y_p}{k_s}\right)\right)^2} \tag{4.15}$$

thus the Shield's parameter can be expressed by:

$$\theta = \frac{\tau_b}{\rho_m \Delta g D} \tag{4.16}$$

The latter gives a formulation for the forces acting on the bed particle, but does not tell us if the particle is moving or not. In order to determine if a particle has undertaken motion or is still at the sand-bed, a second parameter needs to be introduced. The critical Shield's parameter or critical shear is the stability criterion at which particles undertake motion. Brownlie [19], fitted a curve to the experimental values of Shield's. Expression 4.17 is the fit found by Brownlie. This expression is used as a threshold of a particle's motion.

$$\theta_{cr0} = 0.22 {Re'_p}^{-0.6} + 0.06 e^{-17.77 {Re'_p}^{-0.6}} \tag{4.17}$$

Where $Re'_p = \frac{d\sqrt{\Delta g d}}{\nu}$ is a modified particle Reynolds number.

Are available at the moment, an indicator of the state of the forces acting on the bed particles (Shield's parameter) and, a stability criterion (Critical Shield's parameter). The stability criterion as presented in expression 4.17 and expresses the resistance to erosion solely by means of the particle size. Additional resistance to erosion can be included in the stability criterion (θ_{cr0}). In fact, the removal (erosion) or addition (deposition) of sediment to the bed, will produce slopes. Therefore θ_{cr0} has to be corrected to take into account the slope effect. In high speed erosion, a resistance produced by the bulk properties of sand comes into play. To accoun for all this processes, the formulation of the stability criterion is:

$$\theta_{cr} = \theta_{cr0} \left(\theta_{slope} + \theta_{vR} \right) \tag{4.18}$$

Engelund and Fredsøe [20] have proposed the following expression to account for slope effect:

$$\theta_{slope} = \cos\beta \sqrt{1 - \frac{\sin^2\phi \tan^2\beta}{\mu_s^2}} - \frac{\cos\phi \sin\beta}{\mu_s} \tag{4.19}$$

Here ϕ is the angle between the friction velocity vector and the bed steepest slope, β is the slope angle of the bed with respect to the flat bed and μ_s is the static friction coefficient. This correction takes into consideration the slope of the bed and the impact of the flow direction with respect to the slope. This means that if the flow acts against the slope, θ_{cr} is higher. The resistance of bed particles to being picked up is greater. The opposite happens when the fluid acts down the slope, the erosion process is amplified. The critical Shield's parameter depicted above represents the resistance of a particle to get into suspension. For velocities lower than 1-1.5 m/s, the process of erosion is mainly dependent of the particle size. As presented in by F. Bisschop in [1], for higher flow velocities, the bulk properties of sand come into play. Sand, as a bulk material, has a different behaviour to shearing depending on it's porosity, see [3] and [21]. If sand is loosely packed, shearing leads to a decrease in the void ration, this is a contractant behaviour. The inverse, the dilatant behaviour is observed for densely packed sand. In high speed erosion, the sand at the top layer of the sand bed is sheared, leading to an increase in the void ratio, thus creating a hydraulic gradient. The hydraulic gradient over the top layer as defined as van Rhee [3]:

$$i = \frac{|v_e|}{k} \frac{n_l - n_0}{1 - n_l} \tag{4.20}$$

where:
$|v_e|$, is the norm of the vector is the erosion velocity v_e.
n_l, is the maximum porosity or porosity at loose state.
n_0, the bed porosity and A a coefficient.
k, the permeability.

The formulation used to calculate the permeability is the expression of Den Adel (1987)

$$k = \frac{g}{160\nu} D_{15}^2 \frac{(1 - n_0)^3}{n_0^2} \tag{4.21}$$

The correction of the critical Shield's parameter can be expressed as:

$$\theta_{vR} = \frac{|\vec{v}_e|}{k} \frac{n_l - n_0}{1 - n_l} \frac{A}{\Delta} \tag{4.22}$$

Δ, the immerse density.
$A = \frac{1}{1-n_0}$, is used for a continuum approach, $A = \frac{3}{4}$ is used for a single particle.

$$\theta_{cr} = \theta_{cr0}\left(\theta_{slope} + \frac{|\vec{v}_e|}{k}\frac{n_l - n_0}{1-n_l}\frac{A}{\Delta}\right) \tag{4.23}$$

The stability criterion for high speed erosion processes is formulated by θ_{cr} and accounts for the resistance to erosion produced by the particle size, the slope of the sand-bed and the bulk properties of sand. Now that the notion of incipient motion has been explained, let's see how it is implemented in the calculation of the erosion flux.

4.2.3. Erosion

In this work, erosion is referred as the removal of sediment due to the action of viscous and turbulent stresses on the sand-bed. As a matter of fact, if the fluid forces acting on the sand-bed are strong enough, then the grains of sand can get into suspension and be transported by the fluid. Nevertheless, the assessment of the quantity of eroded material has not a well established theoretical background and the complexity of this process has led scientist to search for answers in the empirical formulations as for the Critical Shield's parameter. The erosion process is determined using empirical formulations that are calibrated to experiments and is often represented by a pick-up flux:

$$\Phi = \frac{E}{\rho_s\sqrt{g\Delta D}} \tag{4.24}$$

A formulation of this adimensional pick-up flux is the expression proposed by van Rijn in 1984. Other pick-up functions are depicted in his work [7]:

$$\Phi = 0.00033D_*^{0.3}\left(\frac{\theta - \theta_{cr}}{\theta_{cr}}\right)^{1.5} \tag{4.25}$$

D_* is defined as an adimensional particle diameter: $D_* = d\sqrt[3]{\frac{\Delta g}{\nu^2}}$.
Note in expression 4.25, the presence of the Shield's (θ) and Critical Shield's(θ_{cr}) parameter. The main unknown here is the Shield's parameter. Remark that the higher the velocity of the fluid, the higher the Shield's parameter and the higher the pick up flux is. The mass flux of sediment being withdrawn by the flow is then:

$$E = \rho_s\sqrt{g\Delta D}0.00033D_*^{0.3}\left(\frac{\theta - \theta_{cr}}{\theta_{cr}}\right)^{1.5} \tag{4.26}$$

4.3. Bed-load transport

The bed-load transport account for the transport of sediment close to the bed. As explained in the work of van Rijn [18], the notion of close to the bed has different interpretations. These interpretations have an impact on the phenomena modelled. Einstein [22], considered the bed-load transport to happen in a 2 particles diameter layer above the sediment bed. In this approach, the saltation of particles is accounted in the suspended sediment transport and was followed by Engelund and Fredsøe [20]. Other scientist like van Rijn [18], formulate the bed-load transport as the transport of sediment being dominated by the gravity forces, therefore, incorporating to some extend the saltation of particles. For simplicity, in this work, the bed-load transport is considered to be a 2-D process which makes the approach similar to the formulation of Einstein. The intra bed transfer of matter is model by solving the following expression.

$$\frac{\partial \eta}{\partial t} = \frac{1}{n_0 - 1} - \nabla \cdot \vec{q}_b \tag{4.27}$$

$\vec{q}_b$ represents the bed-load transport rate vector. Expression 4.27, is derived by not considering the erosion and deposition is the Exner equation. This term takes into consideration several transport modes happening at the surface of the sand bed. The transport modes included in the bed-load transport are saltation, rolling of grains of sand and sliding of material. The different modes of bed-load transport, are depedent on the bed shear velocity, in fact, if the Shield's parameter just exceeds the stability criterion, grains of sand will initialize their motion by rolling or sliding along the bed. If the bed shear velocity is increased, the grains of sand are transported by jumps (saltation), the length travelled by the particles during this jumps depends on the bed shear velocity. The components of the bed load transport rate vector are calculated by the expression used by X. Liu [4].

$$q_i = q_0 \frac{\tau_{b,i}}{|\tau_b|} - C|q_0| \frac{\partial \eta}{\partial x_i}, i = 1,2 \tag{4.28}$$

C is a constant with values between 1.5-2.3, accounting for the slope effect on the sediment flux [4]. q_0 is the bed-load transport rate for a flat bed, it can be calculated using the following formula.

$$q^* = \frac{q_0}{\sqrt{Rgdd}} \tag{4.29}$$

q^*, the Einstein number or dimensionless bed-load transport, is calculated using the approach of Engelund and Fredsøe [20].

if $\theta > \theta_{cr}$:

$$q^* = 17.74(\theta - \theta_{cr})[\theta^{\frac{1}{2}} - 0.7\theta_{cr}^{'\frac{1}{2}}]$$

else:

$$q^* = 0$$

Equation 4.28 shows that the horizontal transfer of mass within the bed has a component that is dependent on fluid stresses, τ_b, and a term that depends on the slope of the bed, $\frac{\partial \eta}{\partial x_i}$. In fact, the resisting forces acting on a sand particle can become driving forces if the slope becomes steep enough. To model this effect, a geotechnical approach of slope stability need to be considered. This consideration are left for further studies and can be an extension of the proposed code in this work. The bed-load transport was deactivated in the simulations, even though the equations have been implemented.

5

Numerical implementation of governing equations

In previous chapters, the equations of fluid motion and sediment transport have been formulated. Nevertheless, partial differential equations need to be discretized in order to be solved numerically. The discretization method is discussed in the following section. The fluid motion equations have two unknowns, the velocity and the pressure. The solution of this two quantities is done by uncoupling them by applying the continuity equation to the momentum equation, this is explained in section 5.2.1. In order to have singular solution of the discretized equations, boundary and initial condition must be set. The boundary conditions of the fields are explained further in this section.

5.1. Discretization method: The finite volume method

The discretization method used here to solve the governing equations of erosion/scour is the finite volumes method. The finite volumes method is a method for solving partial differential equations in a discretized space. Let's consider a general conservation law written as:

$$\frac{\partial u}{\partial t} + \nabla \cdot \vec{f}(u) = 0 \tag{5.1}$$

This partial differential equation is the conservation law of a quantity u with $\vec{f}(u)$ being its flux vector. The equation is solved in a computation space V. V is discretized in non overlapping control volumes (v_i) such that:

$$V = \bigcup v_i,\ i = 1, \ldots, n.\ i, n \in \mathbb{N} \tag{5.2}$$

The finite volume method has the advantage that integrating over any volume V, the divergence term becomes a surface integral by applying the divergence theorem.

$$\frac{\partial}{\partial t}\int_V u dV + \int_V \nabla \cdot \vec{f}(u) = \frac{\partial}{\partial t}\int_V u dV + \oint_{\partial V} \vec{f} \cdot \vec{n} d\partial V \tag{5.3}$$

∂V is the closed surface boundary of volume V and $\vec{n}$ is the outward vector normal of surface ∂V. The divergence theorem make it easy to conservatively asses the divergence term as fluxes going in the volume through the closed boundary are equal to the fluxes going out. In order to have an expression of this conservation law for every control volume, let's consider the control volume v_i.

$$\frac{\partial}{\partial t}\int_{v_i} u dv_i + \oint_{\partial v_i} \vec{f} \cdot \vec{n} d\partial v_i \tag{5.4}$$

Having the control volume average of quantity u in volume v_i being equal to:

$$u_i = \frac{1}{v_i}\int_{v_i} u dv_i \tag{5.5}$$

Then, the equation that has to be solved for every control volume is:

$$\frac{\partial u_i}{\partial t} + \frac{1}{v_i}\oint_{\partial v_i} \vec{f}\cdot\vec{n}d\partial v_i = 0 \tag{5.6}$$

if volume v_i is a polyhedron with m faces:

$$\oint_{\partial v_i} \vec{f}\cdot\vec{n}d\partial v_i = \sum_{k=1}^{m} \vec{f}_k\cdot\vec{n}_k \tag{5.7}$$

then the conservation law can be written:

$$\frac{\partial u_i}{\partial t} + \frac{1}{v_i}\sum_{k=1}^{m} \vec{f}_k\cdot\vec{n}_k = 0 \tag{5.8}$$

5.2. Fluid motion

In Openfoam, the finite volume method is implemented for an arbitrarily unstructured mesh [23]. The variables of the NS equations share the same control volume, therefore, the variables are collocated. Figure 5.1, schematizes the collocated arrangement of discretized variables, the velocity $\vec{u}$ and the pressure p in a 2D uniform Cartesian grid. Furthermore, the solution of the equations is done in a Cartesian coordinates system, unchanged over time.

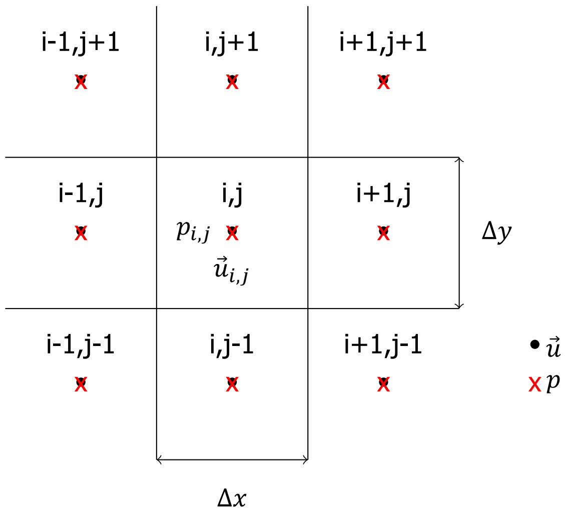

Figure 5.1: Collocated variable arrangement in an uniform 2D Cartesian grid

5.2.1. Pressure-implicit with Separation of Operators (P.I.S.O)

In eq.3.9, there are two unknowns, the velocity field $\vec{u}$ and the pressure field p. Eq.3.9 could be solved simultaneously, but for this work, a segregated approach of the velocity-pressure coupling is used. The P.I.S.O algorithm, proposed by [24] is used for transient calculations. It consists in a predictor step, which gives an estimate of the velocity at the next time step. The first estimate does not satisfy eq.3.8, thus, one or more explicit correction steps are needed to find a suitable solution for eq.3.9.

$$\vec{\nabla}\cdot\vec{u} = 0$$

$$\frac{\partial \vec{u}}{\partial t} + (\vec{u}\cdot\vec{\nabla})\vec{u} = -\frac{\vec{\nabla}p}{\rho} + \nu\nabla^2\vec{u} + \vec{f}$$

In eq.3.9 the advective term $(\vec{u} \cdot \vec{\nabla})\vec{u}$ is not linear. To linearize this term the advective velocity ($\vec{u}$ inside the parenthesis) is taken at the previous time step and the advected velocity as the predicted velocity. The mathematical implementation of this procedure is explained hereafter.

Implicit momentum predictor

A semi-discretized form of eq.3.9 is presented as a linear system:

$$\mathbf{C}\mathbf{u}^* = \mathbf{r} - \nabla\mathbf{p}^\mathbf{n} + \mathbf{g}^\mathbf{n} \tag{5.9}$$

$\mathbf{C}$: is a matrix of coefficients, build from the coefficients multiplying the predicted velocity. The inclusion of viscous or turbulent stresses are made in this matrix.

$\mathbf{u}^*$: the solution array containing the predicted velocities.

$\mathbf{r} = \frac{\mathbf{u}^\mathbf{n}}{\Delta t}$: the right hand side array containing the velocities at the current time step.

$\mathbf{g}^\mathbf{n}$: contains the source term due to the variation of density at time n.

$\nabla\mathbf{p}^\mathbf{n}$: contains the gradient of the pressure at time n.

Solving this implicit linear system will give a prediction of the velocity. As stated previously, $\mathbf{u}^*$ is not divergence free, and one or more corrector steps are needed to find the solution.

Explicit corrector step

Operator $\mathbf{C}$ can be split into 2 matrices. $\mathbf{A}$ its diagonal and $\mathbf{H}'$ its off-diagonal, in other words, $\mathbf{A} + \mathbf{H}' = \mathbf{C}$.

$$\mathbf{A}\mathbf{u}^* + \mathbf{H}'\mathbf{u}^* = \mathbf{r} - \nabla\mathbf{p}^\mathbf{n} + \mathbf{g}^\mathbf{n}$$

Using the predicted velocity $\mathbf{u}^*$, the previous time step $\mathbf{u}^\mathbf{n}$ and the first corrected pressure $\mathbf{p}^*$ we get the expression for the velocity corrector.

$$\mathbf{A}\mathbf{u}^{**} + \mathbf{H}'\mathbf{u}^* = \mathbf{r} - \nabla\mathbf{p}^* + \mathbf{g}^\mathbf{n}$$

if $\mathbf{H} = \mathbf{r} - \mathbf{H}'\mathbf{u}^*$ and $\mathbf{A}$ is inverted, then the linear system yields:

$$\mathbf{u}^{**} = \mathbf{A}^{-1}\mathbf{H} - \mathbf{A}^{-1}\nabla\mathbf{p}^* + \mathbf{A}^{-1}\mathbf{g}^\mathbf{n} \tag{5.10}$$

This equation is the explicit velocity corrector. This expression cannot be determined as no expression for the corrected pressure $\mathbf{p}^*$ has been defined so far. Remember that the corrected velocity should conform to eq.3.8. Therefore, $\nabla \cdot \mathbf{u}^{**} = \mathbf{0}$.

$$\nabla \cdot \mathbf{u}^{**} = \nabla \cdot (\mathbf{A}^{-1}\mathbf{H} - \mathbf{A}^{-1}\nabla\mathbf{p}^* + \mathbf{A}^{-1}\mathbf{g}^\mathbf{n})$$

$$\mathbf{0} = \nabla \cdot (\mathbf{A}^{-1}\mathbf{H} - \mathbf{A}^{-1}\nabla\mathbf{p}^* + \mathbf{A}^{-1}\mathbf{g}^\mathbf{n})$$

and finally:

$$\nabla^2(\mathbf{A}^{-1}\mathbf{p}^*) = \nabla \cdot (\mathbf{A}^{-1}\mathbf{H} + \mathbf{A}^{-1}\mathbf{g}^\mathbf{n}) \tag{5.11}$$

$\nabla^2() = \Delta =$ Laplacian.

This expression is the explicit pressure corrector. The velocity corrector step and the pressure corrector step can be performed several times depending on the accuracy desired. The advantage of this algorithm is that the corrector step can be performed using the same operators. In literature, two corrector steps are enough to reach a "good" accuracy.

5.2.2. Boundary treatment for the velocity

In this work, 2 types of boundary conditions have to be introduced. The Dirichlet boundary conditions are the ones prescribing a value for the fields themselves (pressure, velocity, etc ...). For example, a Dirichlet boundary conditions for the velocity at a boundary with a normal, $\vec{N} = (0, 1, 0)$ can be expressed in the following manner.

$$\vec{u} = (0, a, 0) \tag{5.12}$$

The velocity in the y direction is set to a. The Neumann boundary conditions, in the other hand, are the boundary conditions prescribing a value for the derivative of the fields in question. For example, a Neumann boundary conditions prescribing a zero variation of the velocity in the $\vec{N}$ direction can be expressed in the following manner:

$$\frac{\partial \vec{u}}{\partial \vec{N}} = (0, 0, 0) \tag{5.13}$$

The derivative of every component of the velocity is 0 in the $\vec{N}$ direction.

Walls

The boundary conditions for the velocity at walls, because of the viscous nature of the fluid, is going to be a no slip boundary conditions. This is expressed by the fact that the velocity of the fluid at the boundary is the velocity of the boundary. For a solid not moving wall, the boundary condition is expressed as a Dirichlet boundary condition:

$$\vec{u} = (0, 0, 0) \tag{5.14}$$

This boundary conditions is implemented at the sand bed. This is due to the fact the time step is small and the bed velocity is considered negligible with respect to the fluid velocity. If the bed motion is not negligible then the boundary condition of the velocity should be taken as the velocity of the sand bed.

Inlet

For inlets, the boundary conditions used, is to prescribe the value for the velocity in the direction of the normal of the boundary. For example, in the case of an inlet boundary with a normal, $\vec{N} = (1, 0, 0)$, the value on the velocity is prescribed in the following manner:

$$\vec{u} = (a, 0, 0)$$

or

$$\vec{u}.\vec{N} = a \tag{5.15}$$

a, can be a time dependent value. For the erosion test, an external file prescribing the values at each time step in implemented.

Oulet

The outlet boundary conditions for the velocity is of Neumann type and is mathematically expressed as follows:

$$\frac{\partial \vec{u}}{\partial \vec{N}} = (0, 0, 0) \tag{5.16}$$

With $\vec{N}$ being the normal vector to the boundary. This boundary conditions applied to the advective part of the momentum equation will allow the fluid to 'go out' of the domain as the velocity calculated at the boundary is the same as the one determined at the cells adjacent to the boundary.

5.2.3. Boundary treatment for the pressure

Walls

The boundary condition for the pressure at walls is formulate by a Neumann boundary condition. In fact, the pressure exerted by a wall to the fluid is the reaction of the pressure of the fluid exerted on the wall. Giving the following expression:

$$\frac{\partial p}{\partial \vec{N}} = 0 \tag{5.17}$$

Inlet
For the inlet boundary condition of the pressure:

$$\frac{\partial p}{\partial \vec{N}} = 0 \tag{5.18}$$

Oulet

The boundary condition for the pressure at the outlet is formulated as a constant pressure boundary conditions:

$$p = 0$$

TopWall

The boundary condition for the pressure at the top wall is formulated as a constant pressure boundary conditions. Here:

$$p = 0$$

This allows the pressure to have a singular solution in the settling test.

5.2.4. Boundary treatment for kinetic turbulent energy

Walls

The boundary conditions for the kinetic turbulent energy is derived from wall functions. The wall function for k in foam-extend3.2 is assessed by considering a Neumann boundary condition.

$$\frac{\partial k}{\partial \vec{N}} = 0 \tag{5.19}$$

Outlet

The outlet boundary condition used for k is the same as for the walls.

$$\frac{\partial k}{\partial \vec{N}} = 0 \tag{5.20}$$

Inlet

The inlet boundary condition of k is determined by a Dirichlet boundary condition. The value of k for the inlet is determined using the following formula:

$$k = \frac{3}{2}(UI)^2 \tag{5.21}$$

Where:
U, the bulk inlet velocity.
I, the turbulence intensity, defined as:

$$I = \frac{u'}{< u >} \tag{5.22}$$

Where:
u', the root mean square of turbulence velocity fluctuations.
<u>, the Reynolds averaged velocity.

I is taken as 5% in this work.

5.2.5. Boundary treatment for kinetic turbulent energy dissipation

Walls

ϵ wall function is formulated in the foam-extend framework as :

$$\epsilon = C_\mu^{\frac{3}{4}} \frac{k^{\frac{3}{2}}}{\kappa y_p}$$

if k can be formulated as:

$$k = \frac{u_*^2}{\sqrt{C_\mu}}$$

then

$$\epsilon = \frac{u_*^3}{\kappa y_p} \tag{5.23}$$

The latter expression is used by C. van Rhee, see p. 143 in [6], in this work, the first formulation is used.

Inlet

As for k, the boundary value for ϵ at an inlet is expressed as a Dirichlet boundary condition.

$$\epsilon = C_\mu^{\frac{3}{4}} \frac{k^{\frac{3}{2}}}{l} \tag{5.24}$$

Where l is the mixing length is formulated as:

$$l = 0.5 C_\mu d_h \tag{5.25}$$

with d_h the hydraulic diameter.

Outlet

The outlet boundary condition for ϵ is again of the same type as k.

$$\frac{\partial \epsilon}{\partial \vec{N}} = 0 \tag{5.26}$$

5.2.6. Boundary treatment for turbulent viscosity

Modified sand-bed wall function

In the foam-extend 3.2 framework, the turbulent effect of the flow is included in the Naviers-Stokes equation by the turbulent eddy viscosity in the calculation of the shear stress and is implemented in foam-extend by the expression:

$$\tau_b = \rho_m (\nu + \nu_t) \frac{\partial U}{\partial y} \tag{5.27}$$

From the log law of the wall 4.13 and the definition of the friction velocity 4.14, the shear stress ca be formulated:

$$\tau_b = \frac{\rho_m u_\tau U_p}{\left(\frac{1}{\kappa} ln\left(\frac{32 y_p}{k_s}\right)\right)} \tag{5.28}$$

Discretizing equation 5.27 and equating it to 5.28 leads to:

$$\rho_m(\nu + \nu_t)\frac{U_p - U_b}{y_p} = \frac{\rho_m u_\tau U_p}{\left(\frac{1}{\kappa} ln\left(\frac{32 y_p}{k_s}\right)\right)} \tag{5.29}$$

If $U_b = 0$, then:

$$\nu_t = \frac{y_p u_\tau U_p}{U_p\left(\frac{1}{\kappa} ln\left(\frac{32 y_p}{k_s}\right)\right)} - \nu$$

$$\nu_t = \left(\frac{y_p u_\tau \kappa}{\nu \; ln\left(\frac{32 y_p}{k_s}\right)} - 1\right)\nu$$

y^+ can be expressed in the following way:

$$y^+ = \frac{y_p u_\tau}{\nu}$$

Then the boundary condition of the turbulent eddy viscosity is expressed as follows:

$$\nu_t = \left(\frac{y^+ \kappa}{ln\left(\frac{32 y_p}{k_s}\right)} - 1\right)\nu$$

Wall function

For other walls, the expression used to calculate the boundary value of ν_t, is the default foam-extend implementation which reads:

$$\nu_t = \left(\frac{y^+ \kappa}{ln(E y^+)} - 1\right)\nu$$

here, E=9.8 which is the default value proposed by foam-extend 3.2.

Inlet and Outlet

The boundary values for ν_t are calculated from the values of k and ϵ using the following expression:

$$\nu_t = C_\mu \frac{k^2}{\epsilon} \tag{5.30}$$

5.3. Sediment transport

5.3.1. Implicit solution of sediment transport equation

The term $\frac{\partial c}{\partial t}$ is solved implicitly with a first order forward Euler discretization and $\vec{\nabla} \cdot [c(\vec{v} + \vec{w}_{set})]$ and $\vec{\nabla} \cdot (\nu_t \vec{\nabla} c)$ are solved explicitly and therefore are used as source terms in the solution of $\frac{\partial c}{\partial t}$.

5.3.2. Boundary treatment of sediment transport

Walls

The boundary condition for the concentration at walls is of Neumann type.

$$\frac{\partial c}{\partial \vec{N}} = 0 \tag{5.31}$$

This will disable the diffusion of sediment through the walls. As the velocity at the walls is $\vec{0}$ then no advection is possible.

Inlet

There is no concentration of sediment coming from downstream therefore the boundary conditions is:

$$c = 0 \tag{5.32}$$

Outlet

For the outlet boundary condition for the concentration is that the sediment can go out of the domain if it is transported either by the flow or either the settling of the sediment. The boundary conditions is therefore:

$$\frac{\partial c}{\partial \vec{N}} = 0 \tag{5.33}$$

Sand-bed

For the sand bed boundary conditions, if the sedimentation flux is positive (Deposition of sediment) then the boundary condition is taken as an outflow boundary condition.

$$\frac{\partial c}{\partial \vec{N}} = 0 \tag{5.34}$$

If the sedimentation flux is negative, erosion is present, then, the value of the concentration at the cells adjacent to the boundary is prescribed depending on the balance between the erosion and sedimentation flux.

$$c_i^{k+1} = c_i^k + (E_i)\Delta t \tag{5.35}$$

Boundaries for $\vec{w}_{set}$

For the settling case, $\vec{w}_{set}$ is calculated at the boundaries from the concentration of sediment in the adjacent cell except for the top boundary where the settling velocity is prescribed by a Dirichlet boundary condition.

$$\vec{w}_{set} = \vec{0} \tag{5.36}$$

5.4. Morphological routine and mesh handling

The mesh motion is dependent on the bed elevation. The bed elevation is calculated using the contribution of the sedimentation velocity eq.4.11, accounting for the erosion and the deposition, and the contribution of the bed-load transport, eq.4.27. Once the bed height is calculated at the face center, these face values, are then linearly interpolated to the face vertex, as depicted for a 2-D case in figure 5.2. The mesh point corresponding to the face vertex, is move to the prescribed position (value of the bed elevation at the face vertex). Once this points have been moved, the position of the mesh points in the interior of the domain is calculated by using a laplacian equation explained by H. Jasak and Z. Tuković [25].

$$\nabla \cdot (\gamma \nabla \vec{v}) = 0 \tag{5.37}$$

In this expression γ is the diffusion coefficient and $\vec{v}$ correspond the the grid motion velocity. The new bed position is therefore calculated using:

$$\vec{x}^{k+1} = \vec{x}^k + \vec{v}\Delta t \tag{5.38}$$

$\vec{x}^{k+1}$ and $\vec{x}^k$ are the position vectors at k+1 and k.

The diffusivity used to calculated the grid motion velocity can have different expressions. As presented in [25], the diffusion coefficient can have different values. If the diffusivity is dependent on the inverse of the distance and different laws can be fitted, see table 5.1.

Table 5.1: Diffusion laws for the mesh motion solution

Inverse distance	
linear	$\frac{1}{l}$
Quadratic	$\frac{1}{l^2}$
Exponential	e^{-l}

The distance between the sand-water interface and the pipe-wall under the sand-bed was determined. In order to stop the erosion when the sand-bed has reached the pipe-wall, the Critical Shield's parameter was set to very large number. Setting the Critical Shield's parameter to a large number will stop the erosion process and therefore, the mesh motion.

If $\eta > \eta_{pipe}$

$$\theta_{cr}^{k} = 1e6 \tag{5.39}$$

η is the bed elevation.
η_{pipe} is the elevation at which the pipe is present.

else

$$\theta_{cr}^{k} = \theta_{cr0}\left(\theta_{slope}^{k} + \theta_{vR}^{k}\right) \tag{5.40}$$

Here, the superscripts($k, k-\frac{1}{2}, k-1, k-\frac{3}{2}$...) represent the time at which the values are taken. Furthermore, the correction of the Critical Shield's parameter leads to instabilities if implemented as presented in equation 5.40. In fact, instantaneous small variations of the erosion velocity are amplified with time leading to an erratic behaviour of the model. Let's write the correction of the Critical Shield's parameter as follows:

$$\theta_{vR}^{k} = \frac{|\vec{v}_e^{k-1}|}{k}\frac{n_l - n_0}{1 - n_l}\frac{A}{\Delta} \tag{5.41}$$

Then, in order to stabilize the calculated values of θ_{vR}, it's value at the intermediate time step will be used:

$$\theta_{vR}^{k-\frac{1}{2}} = \frac{\theta_{vR}^{k-1}\frac{\Delta t}{2} + \theta_{vR}^{k}\frac{\Delta t}{2}}{\frac{\Delta t}{2} + \frac{\Delta t}{2}} \tag{5.42}$$

The final implementation of the Critical Shield's parameter corrected for high speed erosion can be formulated as follows:

$$\theta_{cr}^{k} = \theta_{cr}\left(\theta_{slope}^{k} + \theta_{vR}^{k-\frac{1}{2}}\right) \tag{5.43}$$

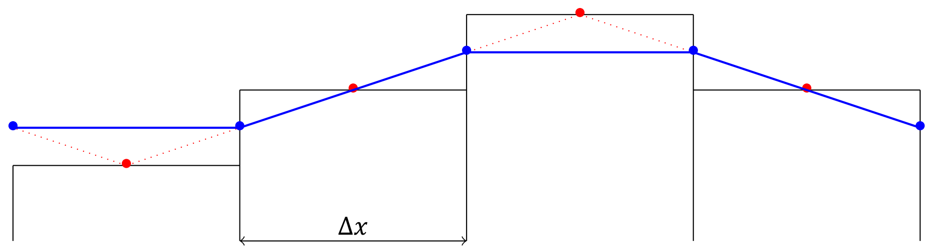

Figure 5.2: Figure representing the calculated bed height at the face centers (Red points), the value linearly interpolated to the edges (blue points) and the actual bed elevation seen by fluid mesh (blue line)

5.4.1. Boundary treatment of mesh motion

TopWall in settling case

The motion of the grid at the upper boundary is 0. Thus the boundary condition is formulated by:

$$\vec{v} = \vec{0} \tag{5.44}$$

Lateral walls in settling case

The mesh slips along the lateral boundaries. The slip boundary condition can be expressed as:

$$\frac{\partial \vec{v}}{\partial \vec{N}} = (0,0,0) \tag{5.45}$$

Sand bed

The motion of the mesh is only prescribed by the bed boundary. Therefore, it is calculated by the sedimentation velocity.

$$\vec{v}.\vec{N} = \vec{v}_{sed}.\vec{N} \tag{5.46}$$

Leading to:

$$\vec{v} = \vec{v}_{sed} \tag{5.47}$$

Remember:

$$\vec{v}_{sed} \cdot \vec{N} = \frac{S - E}{\rho_s(1 - n_0 - c_b)}$$

Boundary condition of the mesh motion at the attachment points of the sand-bed for the high speed erosion case.

For the high speed erosion test, the sand bed is attached to a wall and the outlet boundaries. The boundary condition of the mesh motion at this two locations is an attached point therefore formulated as boundaries of Dirichlet type:

$$\vec{v}.\vec{N} = 0 \tag{5.48}$$

6
Settling test

6.1. Experimental test

Meulenkamp et al. performed one-dimensional settling test, see [6]. This settling test, were carried out with sand presenting the following particle size distribution:

Table 6.1: Particle size distribution

Particle diameter[μm]	76.5	98	115.5	137.5	163.5	194.5	231	302.5
Volume fraction [-]	0.02	0.04	0.15	0.22	0.29	0.2	0.06	0.02

For more information about these tests, the reader is referred to the book cited above. The domain is presented in figure 6.1. The initial dimensions of the fluid domain are 0.282 m width and 1.4m height.

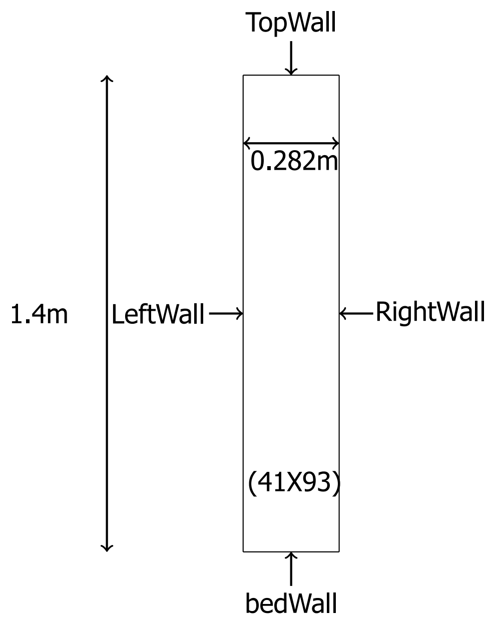

Figure 6.1: Schematized fluid domain for for settling tests

The initial concentration of sediment is considered to be homogeneous with a value of 0.3 and the d_{50} is taken as $150\mu m$. The fluid is initially at rest. The results of the experimental tests are shown in comparison to the simulated results in figures 7.11b, in the next section.

Table 6.2: Simulation parameters

Parameter	ν	ρ_s	ρ_w	g	d_{50}	n_l	n_0
Unit	$[\frac{m^2}{s}]$	$[\frac{kg}{m^3}]$	$[\frac{kg}{m^3}]$	$[\frac{m}{s^2}]$	[m]	[-]	[-]
Value	1e-6	2650	1000	9.81	150e-6	0.55	0.47

6.2. Numerical test

The sand is considered uniform, therefore, the diameter of the particles in the simulation is taken as the d_{50} of the particle size distribution presented in table 6.1.

First, in section 6.2.1, the interaction between the sediment and the fluid is not considered, the Boussinesq approximation is not used. This step will give indication about the behaviour of sediment if considered as a passive scalar in the simulations. If the fluid is considered at rest, the only force acting on the sand particles is gravity, thus, their settling is just described by the hindered settlement velocity formula.

Then, in section 6.2.2, the action of buoyant forces (Boussinesq approach) is included in the calculations. The difference in the local density of the fluid due to presence of sediment will induce the fluid into motion. In fact, the buoyancy induced motion of the fluid will add a new component to the settling of sediment as the fluid will transport the sediment as depicted by the advective term in equation 4.1.

The fields needed to perform the simulation are the following:

- the concentration (c[-])
- the velocity (U[m/s])
- The kinematic turbulent energy (k$[m^2/s^2]$)
- The kinematic turbulent energy dissipation ($\epsilon[m^2/s^3]$)
- the kinematic turbulent viscosity ($\nu_t[m^2/s^1]$)
- the dynamic pressure ($p_{\rho gh}[m^2/s^2]$)
- the mesh point displacement field (displacement[m/s])

This fields, excepted the mesh point displacement field, are initialized in foam-extend as volume fields, this means that the values are defined as the cell averaged quantities located at the cell centers. The mesh point displacement field is defined as displacement of the cell vertex, it is therefore a point field, and is defined as a vectorial quantity. This field is necessary for the computation of the mesh motion and the position at each time step.

6.2.1. Sediment as passive scalar

The contribution for the suspended sediment transport solved in this simulations is:

The sediment transport equation:

$$\frac{\partial c}{\partial t} + \vec{\nabla} \cdot [c(\vec{u} + \vec{w}_{set})] = \vec{\nabla} \cdot (\nu_t \vec{\nabla} c)$$

As the the fluid is considered at rest this equation is reduced to :

$$\frac{\partial c}{\partial t} + \vec{\nabla} \cdot [c\vec{w}_{set}] = \vec{\nabla} \cdot (\nu_t \vec{\nabla} c)$$

The suspended sediment/ bed interaction is fully considered, this means that deposition and erosion are being solved.

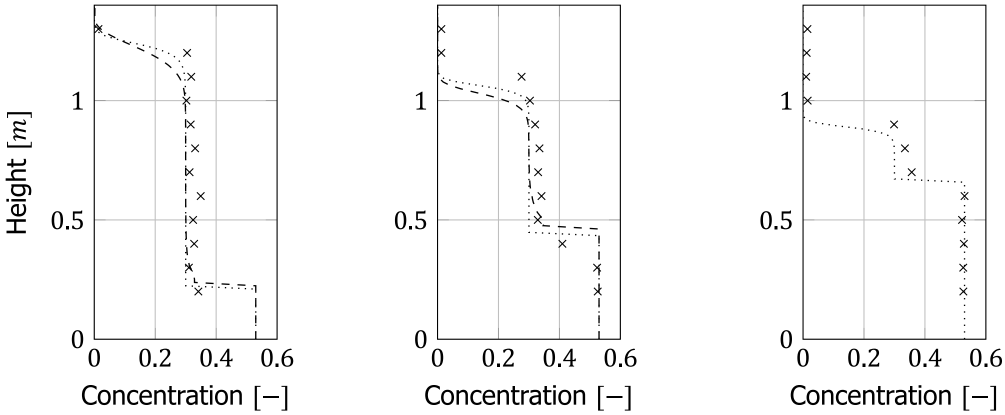

(a) t=50s (b) t=100s (c) t=150s

Figure 6.2: Concentration is a settling test at t=50,100,150s for experimental results(×), simulations results using the Boussinesq approach – – – and omitting this approach(⋯⋯)

Concentration c=0.3

As explained in the introduction of this section, the link between the sediment and the flow motion is not considered. As explained in p.29-30 in the work of C. van Rhee [6], the settlement of sand can be approached with sufficient accuracy by the hindered settlement formula 4.3, because the distance needed for the particles to reach their terminal velocity is in the order of magnitude of the particle's diameter. That is why, particles can be considered to be settling at their terminal settling velocity at t=0s.

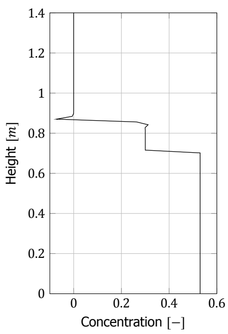

Figure 6.3: Concentration profile for a simulation without Boussinesq aproximation at t=158.887s

In figure 6.2, are plotted the concentration at 50, 100 and 150 seconds. The increase of the sand bed's height in the numerical model can be visualized by the sharp increase of concentration from 0.3 to 0.53, the concentration of the bed. The hindered settling velocity used in the model, depicts the settling velocity of sand as can be seen by the proximity between the calculated and the measured concentrations. The model is not stable after 150s. In fact, for this simulation, the last stable time step is 158.887s. The concentration at this time is presented in figure 6.3.

Mesh motion limit

Note that negative concentration are being calculated in figure 6.3. Other discretization schemes for the advective term in the transport equation and different grid size were tested, leading to the same error. To check the source of this error, a simple simulation of the mesh shrinking was performed. An constant upward motion of the sand-bed boundary was prescribed and set to $1\text{m}.s^{-1}$. The time step size is Δt=1e-4s. The simulation stops at 0.7443s which means that the maximum bed height for this mesh is 0.7443m.

Note that for two consecutive time-steps, the mesh is subjected to an drastic changes. The dark blue zones in figure 6.4 represent zones with very small cells. At t=0.7433s the small cells are located at the middle of the domain. At t=0.7434s, the small cells are present at the top and bottom of the

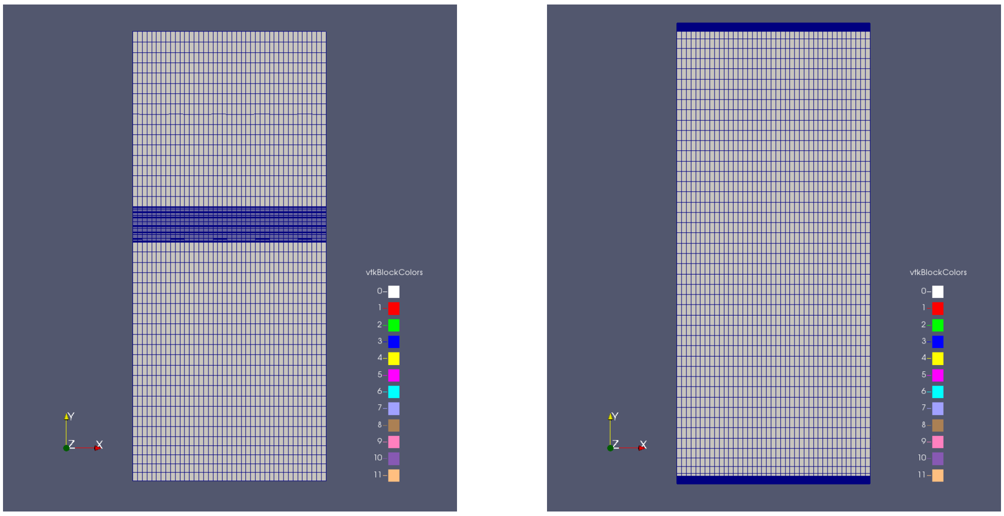

(a) Mesh at t=0.7433s (b) Mesh at t=0.7434s

Figure 6.4: Mesh at 2 consecutive time steps

domain. This instability starts at the mesh motion calculations and is spread to the other fields. The simulation using an initial condition for the concentration of sand in the domain of 0.3, will yield a bed height higher than 0.7924m. As 0.7924m>0.7443m, the simulation will initial concentration of c=0.3 cannot be completed as the mesh calculation do not allow it. Nevertheless, if the initial concentration is c=0.2, the maximum bed height would be 0.5283m<0.7443m. Further in this section, this simulation is performed. The solution to the mesh problem would be to search a new law for the mesh motion or a removal of cells. This is left for further studies.

Concentration c=0.2

Another simulation, this time with an initial concentration c=0.2 is tested. This will prove that the instabilities are not produced by the transport of sediment equation.

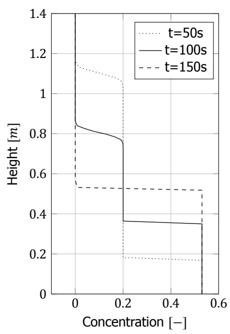

Figure 6.5: Calculated concentration for a settling test at t=50,100,150s for an initial concentration of c=0.2

At t=150s, the concentration in the fluid domain is $5e-6m^3$. This means that the sand has almost completely settled. The calculated bed height at this time step is 0.527974m. These simulations are 2D, nevertheless, a depth needs to be defined in order to perform the calculations (required by OpenFOAM). The depth is z=0.1m, the initial domain height h=1.4m and the width w=0.282, therefore, the volume of sediment contained in the bed is:

$$V_{settled} = \eta\, w\, z\, (1 - n_0) \tag{6.1}$$

The quantity of sediment in the fluid domain is defined is:

$$V_{suspended} = h\, w\, z\, c \tag{6.2}$$

Table 6.3: Volume of suspended sediment and volume of settled sand at 0s and 150s of simulation time

Time [s]	$V_{suspended}[m^3]$	$V_{settled}[m^3]$	$V_{tot}[m^3]$
0	0.007896	0	0.007896
150	0.000005	0.007891	0.007896

Where:
c, the volumetric concentration of sediment.
n_0, the bed porosity, (1-n_0) the bed volumetric concetration of sediment.
η, the bed elevation.
z, the depth of the domain.
w, the width of the domain.
h, the initial height of the domain.
$V_{suspended}$, the volume of suspended sand in the domain.
$V_{settled}$, the volume of settled sand.

At t=150s, the volume of sediment in the fluid domain accounts for $5e-6m^3$ and the volume of settled sand is 0.007891 m^3. The total volume of sand in the system equates the initial volume of suspended sediment. The volume of sediment in the system fluid domain + bed is plotted hereafter.

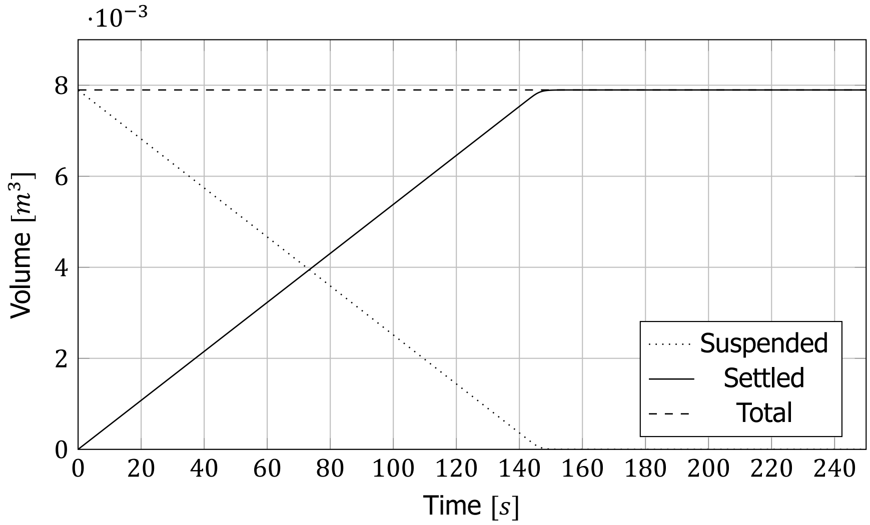

Figure 6.6: Calculated volume of sand settled, suspended and the total during a simulation with initial concentration of c=0.2

As can be seen in figure 6.6, the sediment is conserved during the simulation.
Until the instabilities appear, the simulation with initial concentration c=0.3 is also sediment conservative.

6.2.2. Boussinesq approximation

The contribution for the suspended sediment transport solved in this simulations is:
The sediment transport equation:

$$\frac{\partial c}{\partial t} + \vec{\nabla} \cdot [c(\vec{u} + \vec{w}_{set})] = \vec{\nabla} \cdot (\nu_t \vec{\nabla} c)$$

Here, the fluid is initially considered at rest, nevertheless, the momentum equation accounts for the Boussinesq approximation of the body forces due to the variation of the density of the mixture:

$$\frac{\partial \vec{u}}{\partial t} + (\vec{u} \cdot \vec{\nabla})\vec{u} = -\frac{\vec{\nabla} p}{\rho} + \nu \nabla^2 \vec{u} + \frac{\rho_m - \rho_w}{\rho_w} \vec{g}$$

Density differences will lead the mixture into motion.

Unstable simulation

As stated in previous sections, the Boussinesq approximation is a simplification that neglects all the compressive forces except for the buoyant/gravity forces. The action of this force is mathematically implemented as body forces in the momentum conservation equation. In reality, the momentum exchange between sediment and fluid is a much more complex phenomenon to what the Boussinesq approximation can model. Nevertheless, this approximation was chosen because of its simplicity. Buoyancy forces appear when there is an inhomogeneous distribution of sediment. A higher concentration of sediment yields to a higher density. Heavier fluids tend to sink and lighters rise. In this section, the sedimentation process is study if buoyant forces are considered. Several simulations were performed and this lead to the conclusion that the model as it is defined was not stable. The instabilities find their origin in other reasons than for the non-Boussinesq simulations. The results of unstable simulation are shown hereafter.

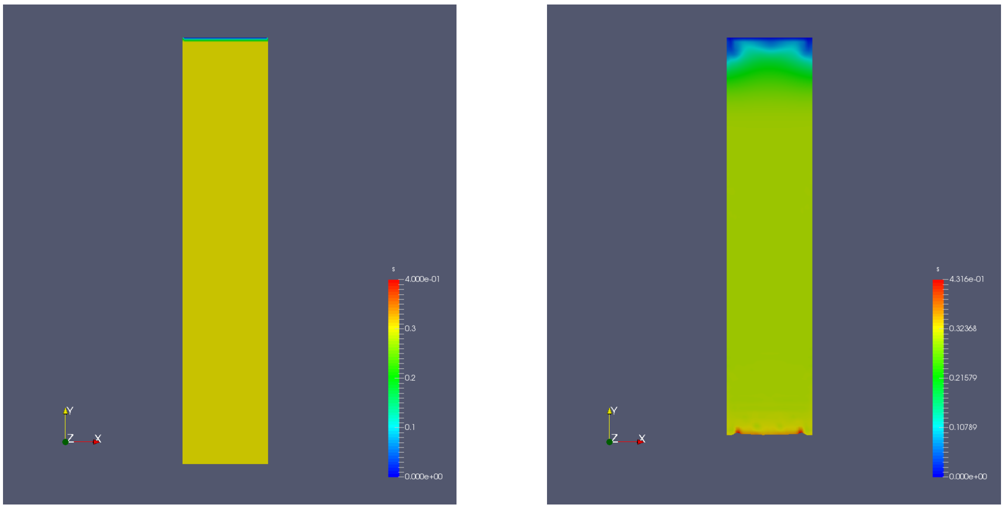

(a) Initial concentration field c=0.3 (b) Concentration field at t=20s

Figure 6.7: Concentration field at different time steps

In figures 6.7, the concentration field (s in the simulations) is presented at t=0s and t=20s. In one hand, subfigure 6.7a depicts the initial concentration field, in the other, subfigure 6.7b shows the field state at t=20s. In the latter, a local increase/decrease of the concentration can be noted in the bottom of the domain. In subfigure 6.7b, it can be seen that the local increase/decrease of the concentration at the bottom of the fluid domain leads to an irregular local sedimentation. The irregular bed height is the proof of this process. This irregular local sedimentation is the root of the instabilities in the simulations using the Boussinesq approach.

As the sediment is settling, the difference in density will yield to a fluid motion. This motion is irregular and will lead to a local increase/decrease of concentration in the vicinity of the sand bed. Figure 6.8 shows the component of the velocity in the x direction. Note that in the lower part of the domain, there is a motion of the fluid from the lateral boundaries towards the center of the domain. The velocity component in the x direction reaches its maximum near the two small dunes that have appeared and then reduce its magnitude towards the center of the domain. In term of sediment transport this leads to an increase of sediment in certain cells. In other words, if a cell is receiving more sediment than what it gives, then the amount of sediment in the cell will increase.

The end result of this instabilities are presented in figure 6.9. This figure shows the magnitude of the velocity field, when the irregular sedimentation is amplified it leads to an unusable mesh. See that the velocity magnitude reaches almost 0.8 $m.s^{-1}$, this velocity magnitude leads to some erosion of the sand bed. Furthermore, the behaviour of the fluid can be derived from figure 6.9. The fluid is try to go up near the center of the domain. As the fluid is coming from the bottom of the domain and it has picked up sand from the bed, the concentration it is carrying is higher than in the surrounding fluid, thus, its density is higher and has to go down near the right boundary.

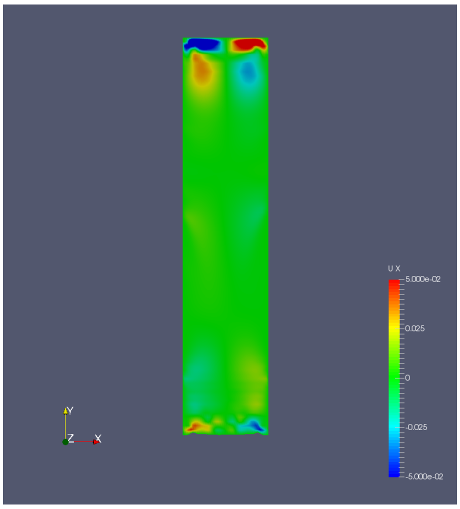

Figure 6.8: Component in the x direction of the velocity at t=20s

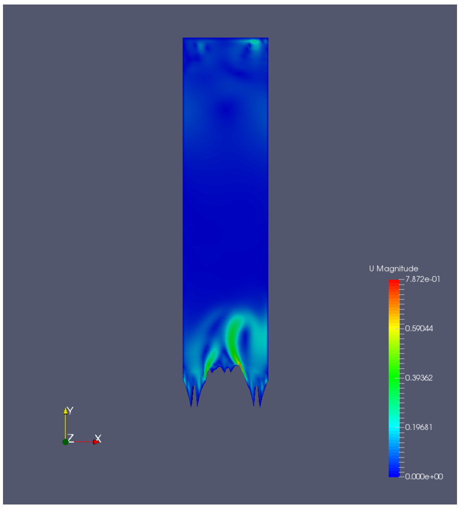

Figure 6.9: Component in the x direction of the velocity at t=66.4s

Stable simulation

In the previous subsection, it has been explained how and why the Boussinesq approximation leads to instabilities in the simulations. In order to achieve a stable solution to the sedimentation problem, the diffusivity near the sand-bed has been increased. It is expected that this increase in the diffusivity coefficient in the sediment transport equation will lead to a smearing of the concentration in the cells above the sand-bed, thus, increasing the homogeneity of the sedimentation process. The transport equation of sediment 4.1 at the cells bordering with the sand-bed will then have a modified diffusivity coefficient in the Laplacian term defined as $K = \nu_t + C_{diff}$. Where C_{diff} is a constant.

Figures 6.10 show that the hypothesis of adding diffusion to the transport equation for the cells in contact with the sand bed smear the concentration and leads to more homogeneous settling. For the simulation using C_{diff}=5e-4, large slopes can be spotted. In the contrary, if C_{diff}=1e-3 then the settling is clearly more uniform. Some gentle slopes are present closer to the boundaries. The initial volume of sand in suspension is $V_{suspended}$=0.007896 m^3. The final calculated volume in the sand bed is $V_{settled}$=0.00790266 m^3. The error done by the model is then err=0.084% of the initial volume of sand.

The settling results using the Boussinesq

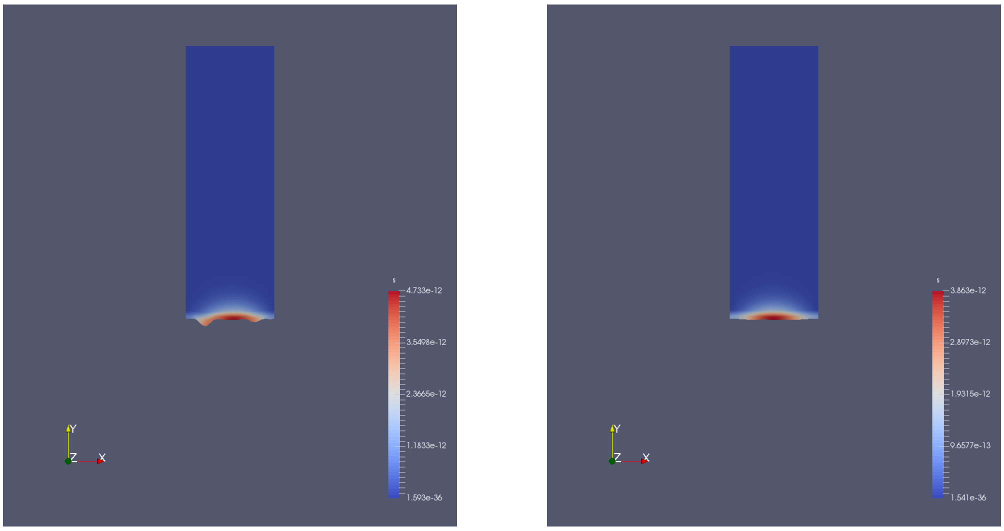

(a) C_{diff}=5e-4 (b) C_{diff}=1e-3

Figure 6.10: Screenshot of the concentration field at t=250s(simulation end) for different values of C_{diff}

6.3. Summary

In section 6.2.1, it was shown that the combination of the formulae for the settling velocity of a single particle, eq.4.2, the hindered settlement velocity, eq.4.3, and the formulation of the exponent by Rowe, eq. 4.6, yield a good approximation of the behaviour of suspended sand, see figures 6.2. In the latter figures, the bed is present when the concentration is c=0.53. The formulation of the sedimentation velocity, eq.4.9, proposed by van Rhee give a conservative assessment of the quantity of sand passing the sand-water interface using the aforementioned approach of the settling of suspended sand.

Section 6.2.1 gave an idea of the limitations of the mesh deformation, and showed that the simulation using an initial concentration of c=0.3 was not stable for very long simulations, see figure 6.2. It is proven by figures 6.4, that the mesh solution get unstable for a certain shrinking of the mesh. This instabilities are responsible for the negative values of the concentration in figure 6.3. The problem does not take its root in the transport equation as simulations using smaller initial concentrations seems to yield good results, see section 6.2.1. A better look at the solution of equation 5.37 should be done in further works.

In section 6.2.2, the buoyancy forces acting on the fluid have been included. These forces lead the fluid into motion yielding an increase of the concentration in cells adjacent to the sand-bed boundary. This increase in concentration will produce localized sedimentation making the mesh unusable after a certain time, see figure 6.9. In order to solve the problem produced by the localized sedimentation, in section 6.2.2, it is proposed to use a constant diffusion coefficient that is added to the eddy turbulent viscosity in the sediment transport equation. This constant coefficient smears the concentration in the cells next to the boundary and the homogeneity of the sedimentation is dependent on the value of the coefficient. Two simulations with different values for the coefficient are presented in figures 6.10.

7

High speed erosion test

7.1. Experimental test

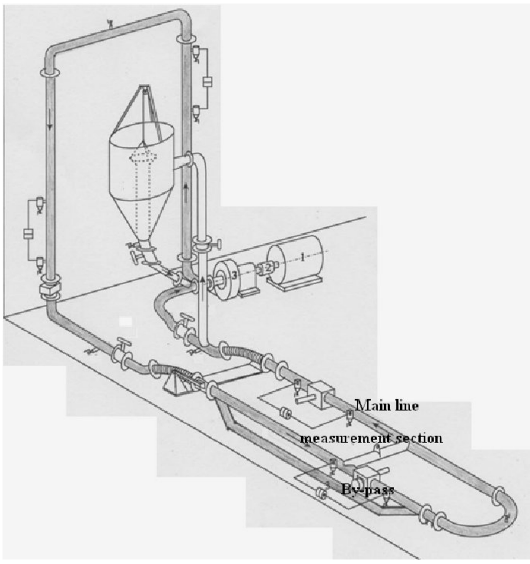

Figure 7.1: Schematic description of the experimental set up used by Bisschop et al.(2015)[1]

High speed erosion tests (HSET) have been performed at the Dredging department of Delft University of Technology. In figure 7.1 the experimental setup present in the Dredging lab of the faculty of Mechanical, Maritime and Materials Engineering (3Me) is depicted.

In this work, a short description of the experimental setup is done, for a full description of the experimental setup, the reader is referred to Bisschop et al.(2015)[1]. The erosion process undergoing in measurement section is depicted in figure A.1. The test in in question for this work is test 54.

Conductivity probes

At $t = 0$ of the HSET, the measurement section has a settled sand-bed. Through the experiment, the sand-bed height is measured by conductivity probes placed in the Lexan window in the measurement section. These probes are used to measure the concentration of sand. The vertical position of the conductivity probes is presented in the following table.

The measurements of concentration by the conductivity probes, are presented in figure 7.2. The conductivity probes measure the concentration of sediment in their vicinity. The concentration measured by the probes for t<2s, is of c=0.55 for probes a-n. Probes o and p measure a concentration of c=0. This means than the sand-bed interface is somewhere in between probe n and o. The sand-bed erosion can be seen by the sudden decrease in concentration for the probes already under the bed

Table 7.1: Vertical position of the concentration probes with respect to the bottom of the measurement section

Probe	a	b	c	d	e	f	g	h
Vertical Height [m]	0.0142	0.0242	0.0342	0.0442	0.0542	0.0642	0.0742	0.0842
Probe	i	j	k	l	m	n	o	p
Vertical Height [m]	0.0942	0.1042	0.1142	0.1242	0.1342	0.1442	0.1742	0.2242

(a-n). Probes o and p read a concentration of sediment for t>2.5s, sediment reaching this 2 probes is due to the effect if the diffusion/ dispersion of sediment.

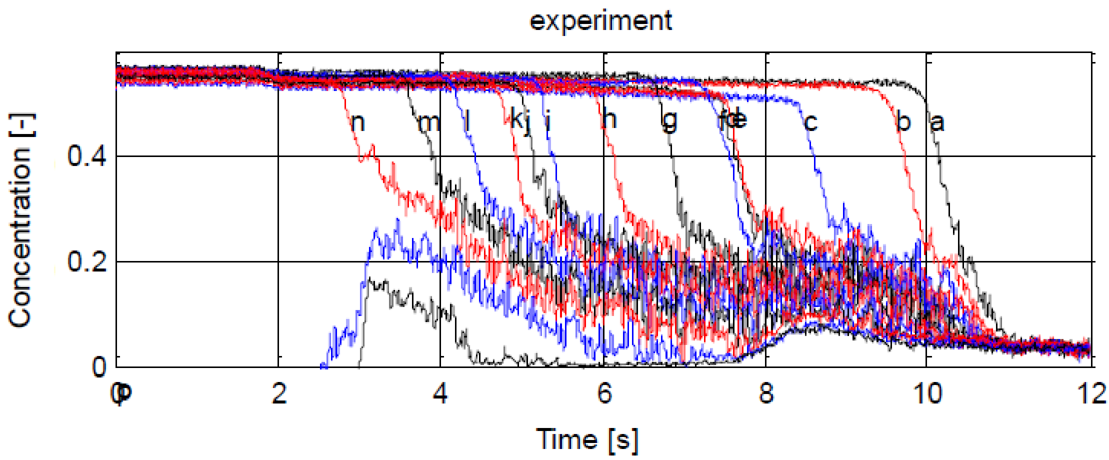

Figure 7.2: Concentration measured by the conductivity probes during the erosion test

Sand properties

The type of sand studied is "Geba" sand with a particle size distribution as shown in table 7.2. The bulk density of "Geba" sand is 1350$kg.m^{-3}$.

Table 7.2: Particle size distribution

Particel diameter[μm]	30	53	75	90	106	125	150	180	212	500
% smaller	0	1.1	3.2	7.8	21.8	49.9	80.2	91	98.5	100

Fluid velocity

The bulk velocities of the fluid in the measurement section are shown in figure 7.3. The 2D numerical experiment will use a domain that is a 1:1 copy of the measurement section. The inlet velocities for the numerical experiment are then to be taken at the entrance on the measurement section. As the experiments are 2D, the height of the measurement section and its entrance can be considered as the area of the section. Therefore, the mass conservation in a pipe can be expressed as the conservation of discharge. U_{inlet} is determined from the conservation of discharge, the dimensions of the measurement section and the velocity in the measurement section $U_{measu.section}$

$$U_{inlet} = 1.92 U_{measu.section} \tag{7.1}$$

U_{inlet} is then calculated from $U_{measu.section}$, the continuous line in figure 7.3. This gives the boundary condition for the inlet velocity in the numerical model and introduces the next section.

7.2. Numerical model setup

In previous sections, we have described the equations governing the erosion process. The fluid motion is modelled using an incompressible P.I.S.O algorithm. The Boussinesq approximation, if implemented, accounts for buoyant forces due to the presence of sediment in the fluid. The van Rijn pick up function will calculate the amount of sediment being suspended by the flow. In order to perform the calculation,

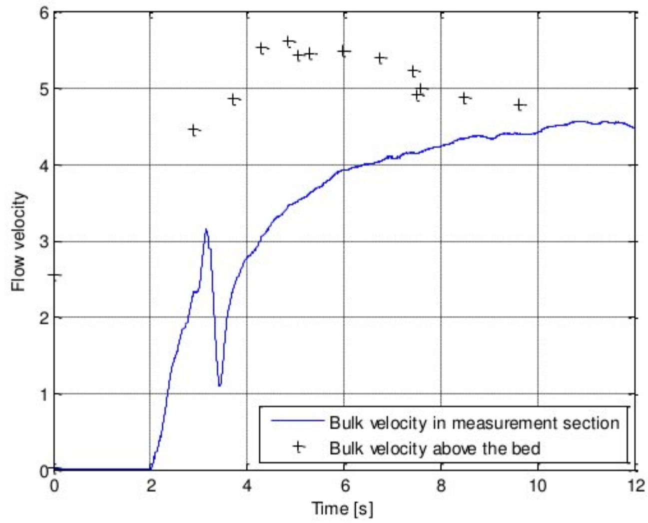

Figure 7.3: Experiments bulk velocities of the fluid for an empty pipe (continuous line) and for a pipe with a sand-bed (+ marks)

Table 7.3: Simulation parameters

Parameter	ν	ρ_s	ρ_w	g	d_{50}	n_l	n_0
Unit	$[\frac{m^2}{s}]$	$[\frac{kg}{m^3}]$	$[\frac{kg}{m^3}]$	$[\frac{m}{s^2}]$	[m]	[-]	[-]
Value	1e-6	2650	1000	9.81	125e-6	0.55	0.45

discretization schemes and boundary conditions are applied to the constitutive relations of flow and sediment transport. In this section, the numerical setup of the model is presented, boundary conditions, experimental setup and further more.

7.2.1. The domain

As stated in section 5.4, the mesh is modified every time step depending on the balance of sediment in the sand-bed. The initial position of the sand-bed is presented in figure 7.4. Note that for the simulations, a 5cm pipe section has been added, see figure 7.4. This addition helps the flow stabilize as a uniform inlet boundary condition is used. The fluid domain is a 1:1 copy of the measurement section presented in figure A.1. The sand-bed height in the middle of the measurement section is set to 0.1445m. The sand-bed porosity is considered to be $n_0 = 0.45$.

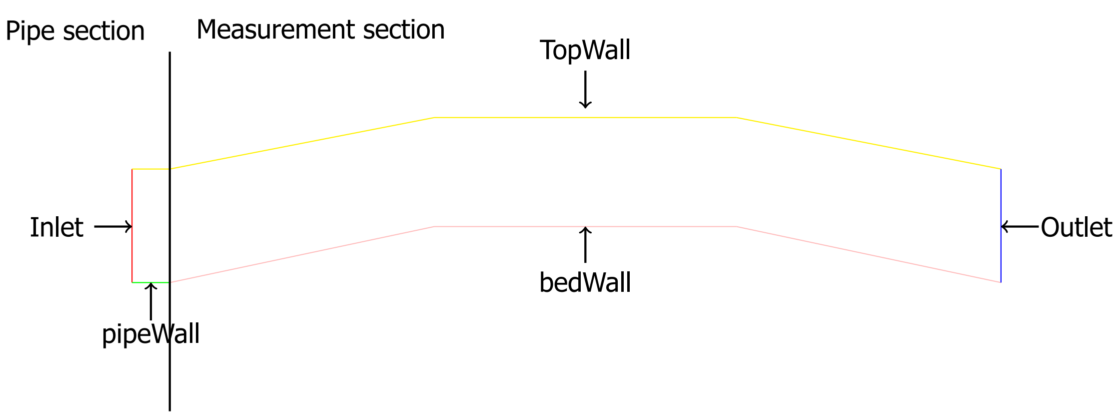

Figure 7.4: Schematized fluid domain for pipe with a sediment bed

The erosion process is blocked by simulation a surface with a very high Critical Shield´s parameter when the sand-bed reaches the position of the pipe wall. The shape of the empty domain is schematized in figure 7.5. In the latter figure, the number of cells at each part of the domain are presented as well.

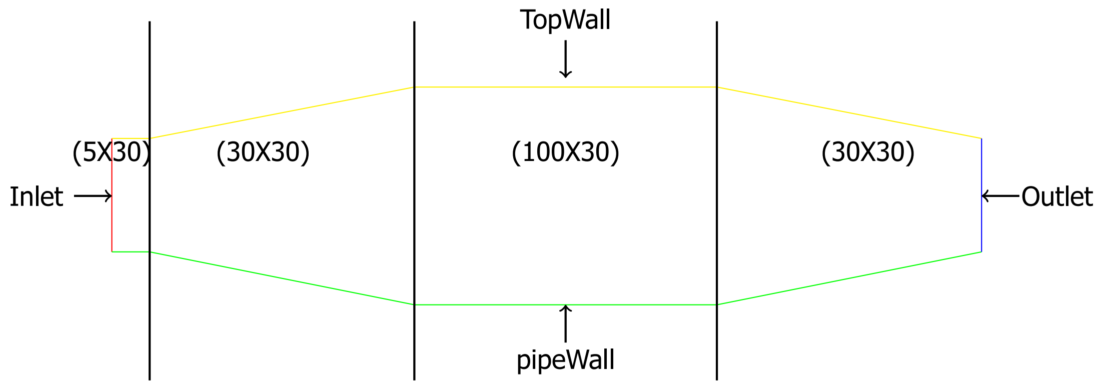

Figure 7.5: Schematized fluid domain for an empty pipe, the number of cells for each part of the pipe are presented as (cells in x direction X cells in y direction)

7.3. Result

7.3.1. Erosion velocity

The high speed erosion, was performed with a $\Delta t = 10^{-4}$. The calibration parameter for this test is the bed roughness (k_s). The condition to choose the value of k_s is that the sand-bed has to be reached the conductivity probe a (see table 7.1) at the same time as the experimental test. Figure 7.2 depicts the measured concentration by the conductivity probes. The probes are reached by the bed, when the measured concentration presents a sudden decrease. In the case of probe a, it is possible to consider that it is reached at $t \approx 10s$. The value of k_s for which probes a is reached at $t \approx 10s$ is $k_s \approx 1.05e-2m$. The bed roughness is introduced by the log law of the wall in the calculation of the turbulent shear stresses and the boundary condition at the sand-bed for the turbulent eddy viscosity.

$$\tau_b = \frac{\rho_m U_p^2}{\left(\frac{1}{\kappa} ln\left(\frac{32 y_p}{k_s}\right)\right)^2} \tag{7.2}$$

As can be seen in the previous formulation, if the bed roughness is lower, then the calculated shear stresses is lower, thus, the erosion velocities is lower and vice-versa.

As state previously, the value of k_s for which probes a is reached at $t \approx 10s$ is $k_s \approx 1.05e-2m$. A comparison of the erosion velocity of the simulation using $k_s \approx 1.05e-2m$ to the experiment and the simulation performed by C. van Rhee is presented in figure 7.6. In comparison the simulation k_s=1.05e-2m, presents higher erosion velocities than the simulation of van Rhee and the experiment of Bisschop [26]. The erosion velocities calculated by the model developed in this work, where calculated by having an output at every $\Delta t = 10^{-2}$s of the concentration at each probe. This could introduced rounding errors in the erosion velocity calculation. The bulk velocity above the bed, was taken as the average velocity seen at probe o, this could be improved by implementing a module in foam-extend 3.2 that could calculate the bulk velocity in a section.

7.3.2. Conductivity probes

After fitting the erosion time in the simulations performed for this thesis with the erosion time measured in the experiments, it is interesting to compare the concentration of sediment measured by the conductivity (figure 7.2) in the experiments and the calculated concentration by the model (figure 7.7). The probes are disposed as presented in figure 7.9.

In these figures, the sand-bed reaching the probes is shown by the sudden drop of the measured concentration. In figures 7.7 and 7.2, between $4s < t < 6s$, an undergoing fast erosion can be seeing. This process becomes slower after this interval. The magnitude of the erosion process can be assessed by the intervals at which the probes are reached by the sand-bed. As seen in figure 7.3, the fluid experience and important acceleration between 3.5s and 6s passing from 1.2 $m.s^{-1}$ to 4 $m.s^{-1}$. The important increase in velocity is responsible for the fast erosion process. After the 6th second, the velocity continues its increase at a slower pace, going from 4 $m.s^{-1}$ to 4.5 $m.s^{-1}$ at the end of the simulation and the experiment, see figure 7.3. In figures 7.7 and 7.2, an increase in the time at which

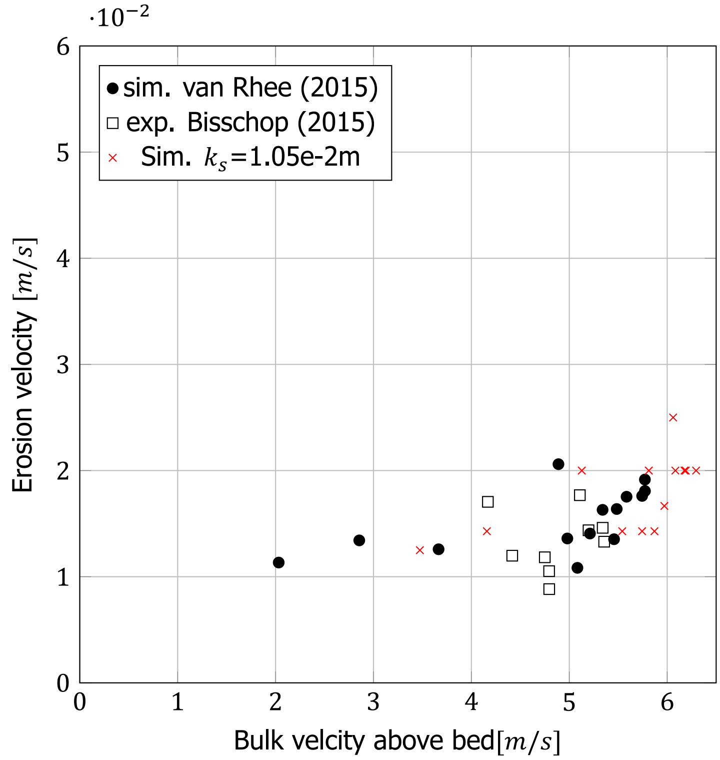

Figure 7.6: Comparison of the erosion velocity between 2 simulations (k_s=1.05e-2m and van Rhee) and the experiments of Bisschop.

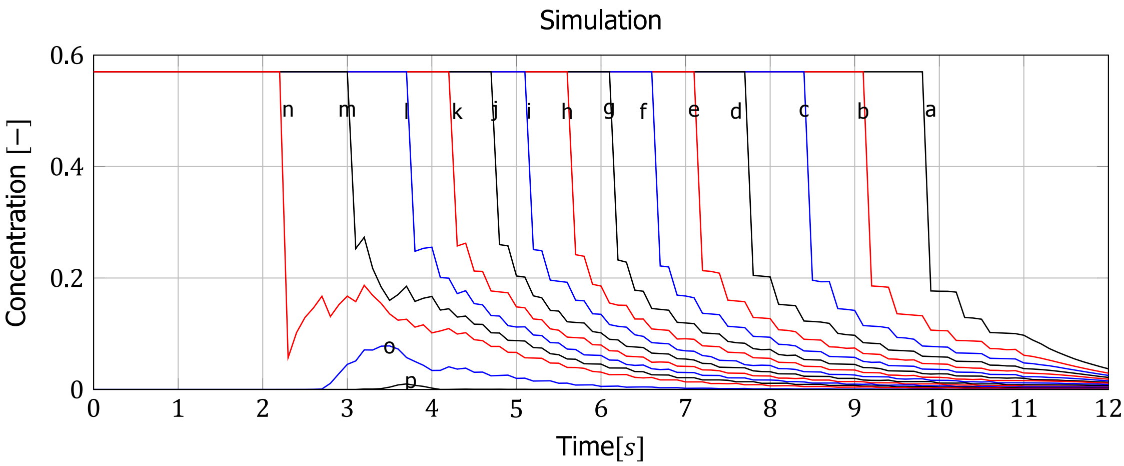

Figure 7.7: Concentration at probes locations over simulation time

probes are reached is presented for t>6s. This shows a slower erosion rate, produced by the reduction of the velocity above the bed due to an erosion induced increase of the hydraulic diameter. The latter statement can be proved by plotting the calculated velocity above the bed and the bulk velocity above the bed determined by the experiment.

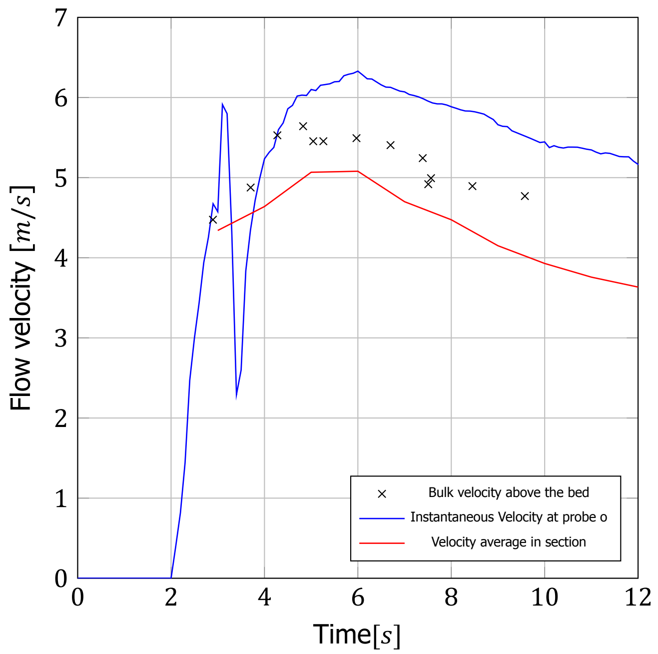

Figure 7.8: Comparison between the bulk velocity above the bed in the experiment and the velocity at probe o in the simulation

7.3.3. Bed height

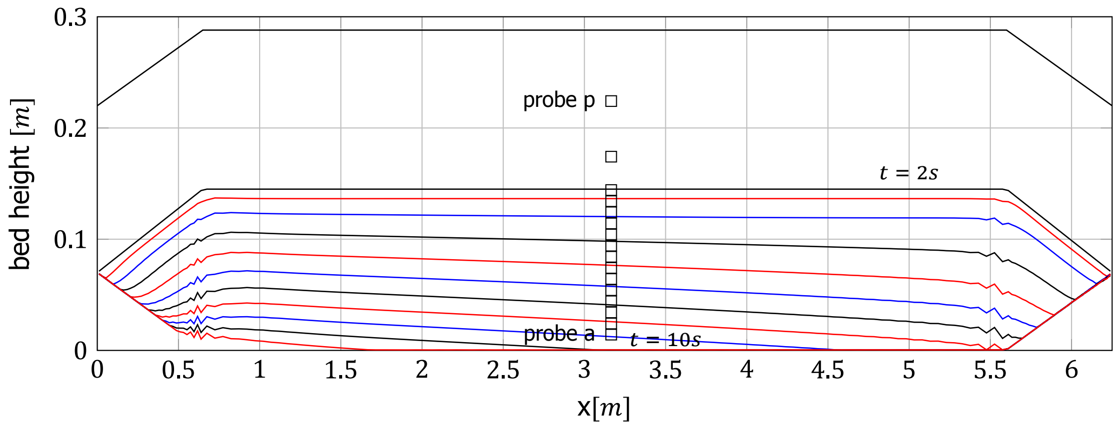

Figure 7.9: Bed height for every second of simulation for t>=2s

In figure 7.9, the side view of the measurement section is shown with the sand-bed height at every second. This figure shows that the hydraulic passage is increased due to the erosion process. Furthermore, it is possible to see some numerical instabilities in the right and left slope. This instabilities have not been studied in detail but their origin seems to be the geometry leading to some velocity fluctuations. Further work should be performed to find the origin of this problem. In figure 7.10, the position of the bed at the position of the probes has been plotted over time. It shows a good correlation between the calculated bed position and the measurements.

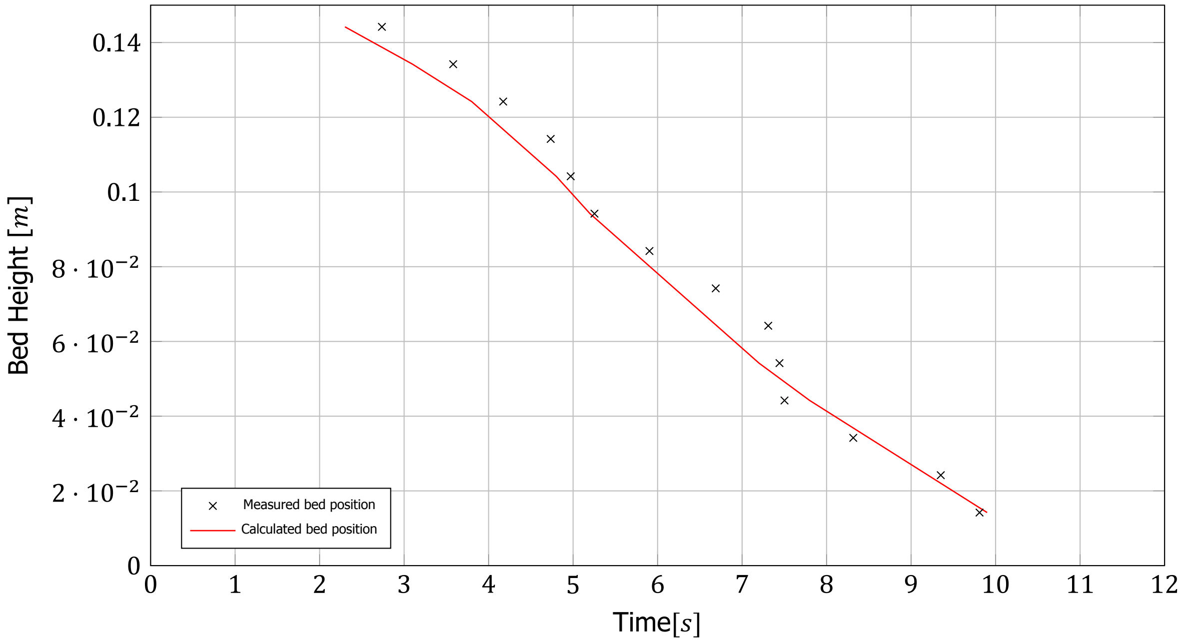

Figure 7.10: Comparison between the measured and calculated position of the bed during the simulation

7.3.4. Velocity, concentration and turbulent eddy viscosity profiles

The profiles of concentration, velocity magnitude and turbulent eddy viscosity are observed at a position x=3.175 of the measurement section.

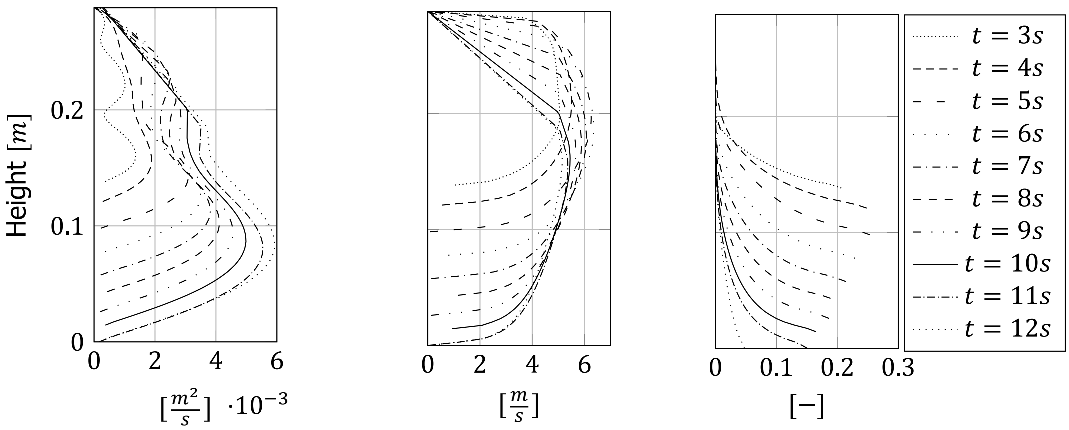

(a) ν_t (b) Velocity Mag. (c) Concentration

Figure 7.11: Turbulent eddy viscosity, velocity and concentration profiles at x=3.175m for every simulation second

In figure 7.11, the section profile of the turbulent eddy viscosity (a), the velocity(b) and the concentration (c) are plotted for every second of simulation. In subfigure (b) the height at which velocities reach zero (the non-slip boundary condition) is the sand-bed height at the simulation time. In subfigure (a), the turbulent eddy viscosity is presented. Remark that the modification of the boundary value of ν_t for the sand-bed is well taken into consideration, the value of ν_t is higher close to the sand-bed. This reduces the velocity of the fluid close to the sand-bed boundary condition, see subfigure (b).

In subfigures (a) and (b) of figure 7.11, the values in the upper cells present a non-accurate behaviour. This behaviour is a result of the automated mesh modifications. In fact, the upper cells present the higher increase ratio. Other laws for the distribution of mesh points were tested leading to similar errors. This distribution law implies that the cells close to the sand-bed will have small deformations. More research should be performed on the mesh deformation module.

The behaviour of the sediment transport module is depicted by subfigure (c). The concentration of sand is higher next to the bed, because, the sand-bed is the source of sediment, the action of gravity and buoyancy incorporated by the Boussinesq approximation and the settling velocity in the transport equation. The concentrations observed in the numerical test of high speed erosion, using the proposed approach, can reach up to 0.25. This range of volumetric concentration should be model using other hypotheses.

7.3.5. Sediment volume conservation

The focus in this subsection is to check that the model does not act as a source or a sink of sediment. In order to verify this, the volume of eroded sediment, the volume of suspended sediment and the volume of sediment leaving the domain, are presented in figure 7.12.

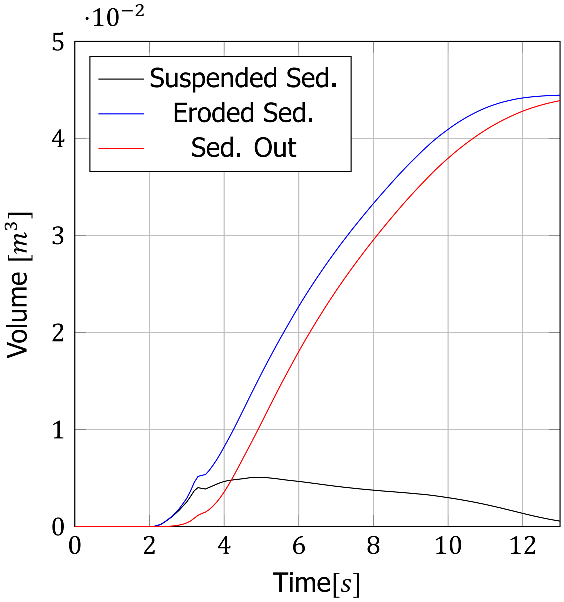

Figure 7.12: Comparison of the cumulative eroded sediment, cumulative suspended sediment leaving the domain through the outlet boundary and the instantaneous suspended sediment in the fluid domain

Between t=2s and t=3s, the sediment is eroded and almost its totality is accounted in the suspended sediment. For t>3s, the sediment is being transported outside of the measurement section. The quantity of sediment being eroded and the quantity leaving the domain seem to balance between 3 and 4.5s maintaining a almost constant volume of sediment in suspension. The suspended sediment reaches its maximum at around 5 seconds, right in the middle of the fastest erosion rates. The volume of sediment in suspension slowly decreases after its peak due to lower erosion rates and the sand leaving the measurement section. Finally the quantity of sediment reaches the quantity of eroded sediment while the volume of suspended sediment tends to 0. The balance of the quantities presented above is presented in figure 7.13. The balance of this quantities is calculated as follows:

$$Vol_{balance} = \frac{Vol_{eroded} - (Vol_{suspended} + Vol_{sed.leavingdomain})}{Vol_{eroded\ at\ sim.end}}$$

The initial volume of sand in the bed is calculated geometrically and yield $0.044506m^3$. The volume eroded at t=13s is $0.0444477m^3$. A small amount of sand is still present after 13s simulation. In figure 7.9, on the bottom left corner of the measurement section, the sand bed has not reached the pipe wall. Figure 7.13 shows the volume balance during the simulation time. The sediment balance error at the end of the simulation is of 0.015%.

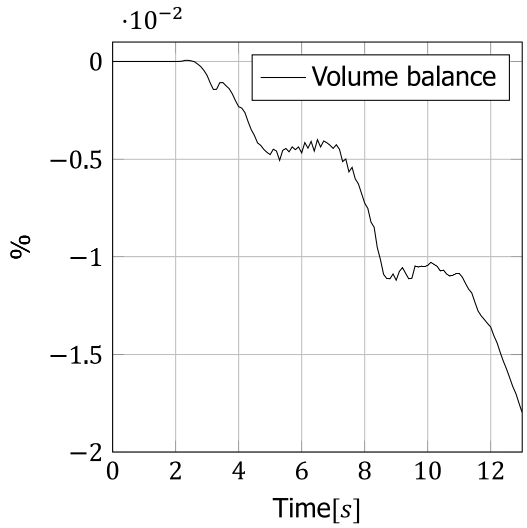

Figure 7.13: Volume difference between eroded material and suspended sediment and sediment leaving the domain by the outlet boundary

8
Conclusion

It is proposed in this work a numerical model of settling and high speed erosion. The model was implemented in the foam-extend 3.2 framework. The solver buoyantBoussinesqPisoFoam was the base solver as it is already a transient incompressible flow solver including the Boussinesq approximation of the buoyancy forces. The equation of the density of the fluid and other modifications of the solver are mathematically depicted in chapters 2 and 3. In chapter 4 is shown the derivation of the modified sand-bed wall function boundary condition for the turbulent eddy viscosity, that was implemented as well. The numerical model proposed for this thesis presents satisfactory results compared to experimental data in settling and erosion modeling. Simulations with different parameters should be compared to experimental data in order to verify the behaviour and accuracy of the model. For the erosion test, the simulated shear stresses are in the same order of magnitude as experimental results. The order of magnitude of the simulated shear stresses is 200 - 300 Pa while test results show shear stresses of 200-600 Pa.

Some limitations are present and some improvements could be done. An example of improvement, is the implementation of smoother inlet boundary condition. In figure 7.8, the instantaneous velocity at probe o are higher than the bulk velocities determined by the tests. Subfigure (b) of figure 7.11, shows the velocity distribuition. The behaviour of the velocity field close to the sand-bed is caused by rough boundary condition implemented via the turbulent eddy viscosity, see subfigure (a). Therefore, the velocity at probe o depends on the distance between the bed and probe o. In figure 7.8, the calculated average velocity shows that the average velocity in the section is lower than the velocity at probe o. This average was done by adding the values using ParaView as an output. It would be more accurate to use length-averaged, and further, face-averaged values for the calculation of the average velocity. As a recommendation, this approach could be implemented. This would help not just for this work but would greatly simplify the comparison between results from foam-extend 3.2 and experimental data.

As seen in figures 7.11, the implementation of the mesh modification presents some limitations concerning the modelling of erosion and deposition of granular material, see section 6.2.1. Further work could be done on better understanding the automated mesh motion. Automatic mesh refinement could be explored.

Discretization schemes other than a limited scheme of the advective term of the sediment transport equation can be tested or even improved.

Bibliography

[1] F. Bisschop, S. Miedema, P. Visser, G. Keetels, and C. van Rhee, *Experiments on the pick-up flux of sand at high flow velocities* (2nd revision, J. of Hydraulic Eng., 2015).

[2] A. Shield, *Anwendung der Ähnlichkeitsmechanik auf die Geschiebebewegung* (Berlin, Preussische Versuchanstalt für Wasserbau und Schiffbau, Mitteilungen, no. 26, 1936).

[3] C. van Rhee, *Erosion of granular sediments at high flow velocity* (Hydrotransport 17, The 17th International Conference on the Hydraulic Transport of Solids, Cape Town, South Africa, 2007).

[4] X. Lui, *Numerical models for scour and liquefaction around object under currents and waves*, Ph.D. thesis (2008).

[5] N. Jacobsen and J. Fredsøe, *A Full Hydro- and Morphodynamic Description of Breaker Bar Development*, Ph.D. thesis (2011).

[6] C. van Rhee, *On the sedimentation process in a Trailing Suction Hopper Dredger* (Ph.D. Thesis, Delft University of Technology, 2002).

[7] L. van Rijn, *Sediment pick-up functions* (Journal of Hydraulic Engineering, ASCE, No. 10, 1984).

[8] P. Wesseling, *Principles of Computational Fluid Dynamics* (Secaucus, NJ, USA:Springer-Verlag New York, Inc, 2000).

[9] J. Goeree and C. van Rhee, *Numerical sediment simulation using a continuous flow model* (16th International Conference on Multiphase Production Technology, 12-14 June, Cannes, France, 2013).

[10] B. M. Sumer, H. Jensen, Y. Mao, and J. Fredsøe, *Effect of lee-wake on scour below pipelines in current* (J. Waterway, Port, Coastal, Ocean Eng., 114(5), 1988).

[11] B. M. Sumer, L. Chua, N. S. Cheng, and J. Fredsøe, *Influence of turbulence on bed load sediment transport* (Journal of Hydraulic Engineering, ASCE , 129(8), 585-596, 2003).

[12] R. Ferguson and M. Church, *A Simple Universal Equation for Grain Settling Velocity* (Journal of Sedimentary Research 74(6):933-937, 2004).

[13] J. Richardson and W. Zaki, *Sedimentation and fluidisation. Part 1.* (Trans. Inst. Chem. Eng.32:35-53, 1954).

[14] S. Mirza and J. Richardson, *Sedimentation of suspensions of particles of two or more sizes* (Chemical Engineering Science Volume 34, Issue 4, 1979, Pages 447–454, 1979).

[15] P. Rowe, *A convenient empirical equation for estimation of the Richardson–Zaki exponent* (Chem. Eng. Sci. 43, 1987).

[16] F. Exner, *Zur physik der dunnen* (Akad. Wiss. Wien Math. Naturwiss. Klasse,129(2a), 1920).

[17] F. Exner, *Uber die wechselwirkung zwischen wasser undgeschiebe in flussen* (Akad. Wiss. Wien Math. Naturwiss. Klasse,134(2a), 1925).

[18] L. van Rijn, *Sediment Transport, Part I: Bed load transport* (Journal of Hydraulic Engineering, ASCE, No. 10, 1984).

[19] W. Brownlie, *Prediction of flow depth and sediment discharge in open channels* (W. M. Keck Laboratory of Hydraulics and Water Resources Report, 43A. California Institute of Technology , Pasadena, CA., 1981).

[20] F. Engelund and J. Fredsøe, *A sediment transport model for straight alluvial channels* (Nordic Hydrology, 7:293-306, 1976).

[21] C. van Rhee, *Sediment entrainment at high flow velocity, Journal of Hydraulic Engineering* (ASCE, vol. 136, no. 9, pp. 572-582, 2010).

[22] H. Einstein, *The bed-load function for sediment transportation in open channel flow* (United States Department of Agriculture, Washington, D.C, Technical Bulletion No. 1026, 1950).

[23] H. Jasak, *Error Analysis and Estimation for the Finite Volume Method with Applications to Fluid Flows* (Ph.D. thesis, University of London, 1996).

[24] R. Issa, *Solution of the implicitly discretized fluid flow equations by operator-splitting* (J. Comp. Physics, 62:40–65, 1986).

[25] H. Jasak and Z. Tuković, *Automatic mesh motion for the unstructured finite volume method* (Transactions of FAMENA, 30(6): 1-18, 2007).

[26] C. van Rhee and R. Bisschop, *Numerical Simulation of High-Speed Sediment Entrainment* (17th conference of transport and sedimentation of solid particles, sept 22-25, 2015, Delft, The Netherlands, 2015).

A

Apendix A

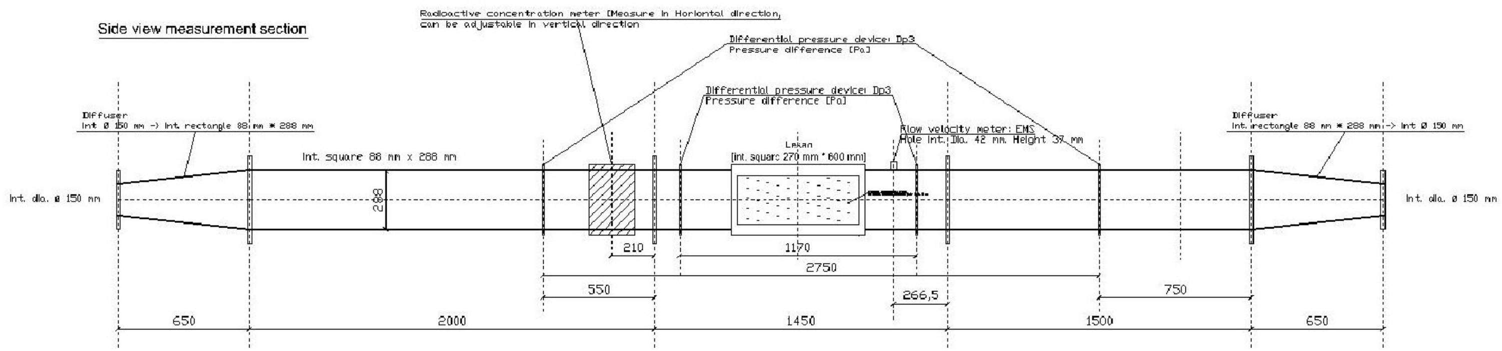

Figure A.1: Side view of the measurement section